

Higher-order topological superconductivity of spin-polarized fermions

Junyeong Ahn^{1,2,3} and Bohm-Jung Yang^{1,2,3,*}

¹Center for Correlated Electron Systems, Institute for Basic Science (IBS), Seoul 08826, Korea

²Department of Physics and Astronomy, Seoul National University, Seoul 08826, Korea

³Center for Theoretical Physics (CTP), Seoul National University, Seoul 08826, Korea

We study the superconductivity of spin-polarized electrons in centrosymmetric ferromagnetic metals. Due to the spin-polarization and the Fermi statistics of electrons, the superconducting pairing function naturally has odd parity. According to the parity formula proposed by Fu, Berg, and Sato, odd-parity pairing leads to conventional first-order topological superconductivity when a normal metal has an odd number of Fermi surfaces. Here, we derive generalized parity formulae for the topological invariants characterizing higher-order topology of centrosymmetric superconductors. Based on the formulae, we systematically classify all possible band structures of ferromagnetic metals that can induce inversion-protected higher-order topological superconductivity. Among them, doped ferromagnetic nodal semimetals are identified as the most promising normal state platform for higher-order topological superconductivity. In two dimensions, we show that odd-parity pairing of doped Dirac semimetals induces a second-order topological superconductor. In three dimensions, odd-parity pairing of doped nodal line semimetals generates a nodal line topological superconductor with monopole charges. On the other hand, odd-parity pairing of doped monopole nodal line semimetals induces a three-dimensional third-order topological superconductor. Our theory shows that the combination of superconductivity and ferromagnetic nodal semimetals opens up a new avenue for future topological quantum computations using Majorana zero modes.

Introduction.— Recently, odd-parity superconductivity has received great attention due to its potential to realize topological superconductors (TSCs) [1–5]. Fu and Berg [6], and also Sato [7, 8] proposed a simple but powerful parity formula relating the parity configuration in the normal state and the topological property of the odd-parity superconducting state. The simplicity of the formula allows a fast diagnosis of the topological nature of a superconducting state by just counting the number of Fermi surfaces, which greatly facilitates the search for TSCs in centrosymmetric materials.

One limitation of the Fu-Berg-Sato formula is that it can be applied only to conventional first-order TSCs in which d -dimensional bulk topology supports gapless Majorana states on $(d - 1)$ -dimensional boundaries. However, recent studies on topological crystalline phases have uncovered higher-order TSCs whose d -dimensional bulk topology protects gapless Majorana fermions on the boundaries with dimensions lower than $(d - 1)$ [9–14]. In general, k th-order TSCs in d dimensions host $(d - k)$ -dimensional boundary Majorana states. In the case of d th-order TSCs in d dimensions, Majorana zero modes (MZMs) exist at the corners, which can be potentially useful for topological quantum computations [2–5].

Up to now, several interesting ideas have been proposed to realize 2D second-order TSCs in various different settings, such as using the superconducting proximity effect on quantum Hall insulators [15], quantum spin Hall insulators [13, 16, 17], second-order topological insulators [18], Rashba semiconductors [19] and nanowires [20]; breaking time reversal symmetry of TSCs with helical Majorana edge states by applying external magnetic field [9, 21–24] or attaching antiferromagnets [25]; and some other ideas [13, 23, 26–28]. In 3D, on the other hand, there are only few mechanisms proposed for realizing a third-order TSC such as applying

magnetic field to a 3D second-order TSC with helical hinge modes [9]. For more systematic investigations of higher-order TSCs, a simple criterion for diagnosing higher-order band topology, similar to the Fu-Berg-Sato parity formula for first-order TSCs, is highly desired. Although some formulae for higher-order TSCs having gapless boundary states were proposed recently [29], the parity formula for d th-order TSCs hosting MZMs is still lacking.

In this paper, we establish generalized parity formulae for higher-order TSCs and apply them to ferromagnetic metals where odd-parity superconductivity naturally arises. Using the generalized parity formulae, we classify all possible spin-polarized band structures of centrosymmetric ferromagnetic metals that can realize inversion-protected higher-order TSC. From this analysis, we find doped ferromagnetic nodal semimetals as an ideal normal state that realizes higher-order TSCs. Explicitly, in 2D, odd-parity pairing of a doped Dirac semimetal (DSM) induces a 2D second-order TSC. In 3D, odd-parity pairing of a doped nodal line semimetal (NLSM) generates a nodal line superconductor with monopole charges. Furthermore, in the case of a doped monopole NLSM [2, 30], odd-parity pairing induces a 3D third-order TSC. These findings show that the combination of superconductivity and spin-polarized 2D and 3D nodal semimetals can be promising platforms for topological quantum computations using MZMs.

Symmetry and nodal structures.— Let us first clarify the symmetry of the normal and superconducting states of ferromagnetic metals with inversion symmetry P_0 and classify the relevant nodal structures. We assume that an electron's spin is polarized along the z -direction. Also, we neglect spin-orbit coupling, but its influence is discussed later. In this setting, although time reversal symmetry $\mathcal{T} = i\sigma_y K$ is broken, the ferromagnetic metallic state is symmetric under the effective time reversal $T \equiv e^{i\pi\sigma_y/2}\mathcal{T} = K$ defined as the product of \mathcal{T} and a 180° spin rotation around the y axis, $e^{i\pi\sigma_y/2}$. Here σ_y is a Pauli matrix for spin degrees of freedom, and K denotes

* bjyang@snu.ac.kr

the complex conjugation operator. Also, $P_0 = P_0^*$ because $[P_0, T] = 0$. Then, the system is invariant, locally at each momentum \mathbf{k} , under $P_0 T$ symmetry satisfying $(P_0 T)^2 = 1$. Such a $P_0 T$ symmetric system belongs to the \mathbf{k} -local symmetry class $\text{AI} + \mathcal{I}$ proposed by Bzdusek and Sigrist [1], where the 1D and 2D topological phases are classified by Z_2 invariants [1, 30]. Here the 1D Z_2 invariant is the quantized Berry phase, which is the topological charge of 2D Dirac points and also of 3D nodal lines. The 2D Z_2 invariant is the monopole charge of 3D nodal lines.

To describe the superconducting state, we introduce a 2N-component Nambu spinor $\hat{\Psi}(\mathbf{k}) = [\hat{c}_{\uparrow\alpha}(\mathbf{k}), \hat{c}_{\uparrow\beta}^\dagger(\mathbf{k})]^T$, where $\hat{c}_{\uparrow\alpha}(\mathbf{k})$ [$\hat{c}_{\uparrow\alpha}^\dagger(\mathbf{k})$] is an electron creation [annihilation] operator with spin up and the orbital index $\alpha = 1, \dots, N$. The corresponding Bogoliubov-de Gennes (BdG) Hamiltonian can be written as $\hat{H} = \hat{\Psi}^\dagger H_{\text{BdG}} \hat{\Psi}$, where

$$H_{\text{BdG}} = \begin{pmatrix} h(\mathbf{k}) & \Delta(\mathbf{k}) \\ \Delta^\dagger(\mathbf{k}) & -h^T(-\mathbf{k}) \end{pmatrix}. \quad (1)$$

Here, $h(\mathbf{k})$ indicates the Hamiltonian for the normal state, and the pairing function $\Delta_{\alpha\beta}(\mathbf{k})$ with orbital indices α, β satisfies $\Delta_{\alpha\beta}(\mathbf{k}) = -\Delta_{\beta\alpha}(-\mathbf{k})$ because of the Fermi statistics of electrons. Since the pairing function forms an irreducible representation of the symmetry group, it can have either odd-parity $P_0 \Delta(\mathbf{k}) P_0^{-1} = -\Delta(-\mathbf{k})$ or even-parity $P_0 \Delta(\mathbf{k}) P_0^{-1} = +\Delta(-\mathbf{k})$.

In the weak-pairing limit, we can focus on the pairing at the Fermi energy E_F and define the corresponding pairing function as $\Delta_{E_F}(\mathbf{k})$. Then, $P_0 \Delta_{E_F}(\mathbf{k}) P_0^{-1} = \Delta_{E_F}(\mathbf{k})$ because Δ_{E_F} is a 1×1 matrix. The Fermi statistics $\Delta_{E_F}(\mathbf{k}) = -\Delta_{E_F}(-\mathbf{k})$ naturally shows that the pairing function satisfies the odd-parity condition

$$P_0 \Delta_{E_F}(\mathbf{k}) P_0^{-1} = -\Delta_{E_F}(-\mathbf{k}). \quad (2)$$

Therefore, in Eq. (1), we consider only odd-parity pairing functions that satisfy $P_0 \Delta(\mathbf{k}) P_0^{-1} = -\Delta(-\mathbf{k})$ (See also the Supplemental Material [33]). The corresponding odd-parity BdG Hamiltonian is symmetric under inversion $P = \tau_z P_0$ which anticommutes with the particle-hole symmetry $C = \tau_x K$, where $\tau_{x,y,z}$ are Pauli matrices for the Nambu space. PT and CP symmetries satisfying $(PT)^2 = 1$ and $(CP)^2 = -1$, which show that the BdG Hamiltonian belongs to the \mathbf{k} -local symmetry class $\text{CI} + \mathcal{I}$ [1]. In this class, 2D Dirac points or 3D nodal lines can be protected as in the case of the class $\text{AI} + \mathcal{I}$. The only difference is that the 1D invariant is integer-valued in the class $\text{CI} + \mathcal{I}$, but this is irrelevant in our analysis below because we are only interested in the parity of the 1D invariant that can be related to the eigenvalues of P .

Nodal structure of TSC and parity formula.— According to Eq. (2), an odd-parity pairing function $\Delta(\mathbf{k})$ changes its sign on the Fermi surfaces surrounding a time-reversal-invariant momentum (TRIM) so that an even number of nodes should appear at the points where the sign of $\Delta(\mathbf{k})$ changes. The number of nodal points can be related with the inversion parities of occupied bands using the idea proposed in Refs. [6–8] as follows. In 2D, the parity of the number of Dirac node pairs related by inversion can be counted by the Z_2 invariant

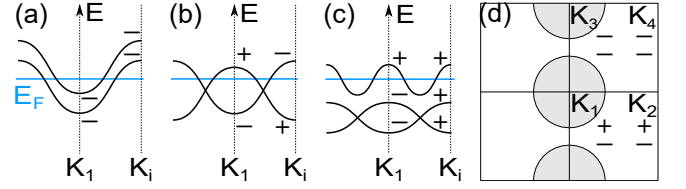


FIG. 1. Band structure and parity configuration of spin-polarized metals leading to 2D second-order TSCs in the weak pairing limit. (a) Two electron-like (or hole-like) Fermi surfaces surrounding the same TRIM. (b) Doped DSM with $\nu_1 = 1$. (c) Normal state whose whole bands, including both occupied and unoccupied bands, have the higher-order topology with $\nu_2 = 1$. The horizontal axes in (a,b,c) schematically represent the 2D Brillouin zone: $\mathbf{K}_1 = (0, 0)$, and \mathbf{K}_i indicates the other three TRIMs with the same parity configuration. \pm represents the parity at TRIM. (d) The fourth way to obtain the higher-order TSCs. Here, the \pm sign on the top (bottom) row at each TRIM represents the parity of the higher-energy (lower-energy) states. One (no) band is occupied in the gray (white) regions, and the boundaries show the relevant Fermi surfaces.

$\nu_1 \equiv \sum_{\mathbf{K} \in \text{TRIM}} n_-^o(\mathbf{K}) \pmod{2}$ [34], where $n_-^o(\mathbf{K})$ is the number of occupied states with negative parity at \mathbf{K} . Here ν_1 can be understood as the number of band inversions at TRIM that create pairs of Dirac points, starting from the trivial phase with only positive-parity occupied states.

One can define a similar parity index ν_1^{BdG} for the BdG Hamiltonian as

$$\begin{aligned} \nu_1^{\text{BdG}} &\equiv \sum_{\mathbf{K} \in \text{TRIM}} n_-^{\text{BdG};o}(\mathbf{K}) \\ &= \sum_{\mathbf{K} \in \text{TRIM}} n_-^o(\mathbf{K}) + n_+^u(\mathbf{K}) \\ &= \sum_{\mathbf{K} \in \text{TRIM}} n^u(\mathbf{K}) \pmod{2}, \end{aligned} \quad (3)$$

where $n_{\pm}^{o(u)}$ is the number of occupied (unoccupied) states with \pm parity in the normal state, $n^u = n_+^u + n_-^u$, and $n_{\pm}^{\text{BdG};o(u)}$ is defined similarly for the BdG Hamiltonian with an odd-parity pairing function. The second line in Eq. (3) results from the odd-parity pairing, and the third line follows from $n_-^o(\mathbf{K}) = n_-^o(\mathbf{K}) + n_+^u(\mathbf{K}) - n_-^u(\mathbf{K}) = n_-^o(\mathbf{K}) + n_+^u(\mathbf{K}) + n_-^u(\mathbf{K}) \pmod{2}$ together with $\sum_{\mathbf{K}} n_-^o(\mathbf{K}) = 0 \pmod{2}$ following from that, when all the bands are occupied, no band crossing exists at the Fermi level. Equation (3) shows that $\nu_1^{\text{BdG}} = 1 \pmod{2}$ only when there exists an odd number of Fermi surfaces. This is consistent with the odd-parity condition of the pairing function $\Delta(\mathbf{k})$ on the Fermi surface in Eq. (2), which guarantees an odd number of Dirac node pairs in the superconducting state per each normal state Fermi surface enclosing a TRIM.

Generalized parity formula for second-order TSC in 2D.— To derive the condition for higher-order superconductivity of spin-polarized electrons, let us introduce generalized parity formulae. According to the Dirac Hamiltonian formalism for inversion-protected higher-order topological phases [9, 35], we can obtain a higher-order TI by inverting 2^n bands at a TRIM starting from a topologically trivial phase. Here, n de-

notes a nonnegative integer. Therefore, counting the number of the simultaneous inversion of 2^n bands at TRIM leads to the following Z_2 index,

$$\nu_{2^n} \equiv \sum_{\mathbf{K} \in \text{TRIM}} \left[\frac{n_-^o(\mathbf{K})}{2^n} \right]_{\text{floor}} \mod 2, \quad (4)$$

where $[m + a]_{\text{floor}} = m$ for an integer m and $0 \leq a < 1$. We can also introduce similar indices $\nu_{2^n}^{\text{BdG}}$ for the BdG Hamiltonian by replacing $n_-^o(\mathbf{K})$ by $n_-^{\text{BdG};o}(\mathbf{K})$. These indices characterize higher-order TSCs.

Let us first discuss the physical meaning of ν_2^{BdG} in 2D. Recently, it was shown that $\nu_2 = 1$ indicates the second-order topology of a PT -symmetric topological insulator with chiral symmetry, characterized by fractional corner charges on the boundary [35–37]. A straightforward extension of this idea shows that $\nu_2^{\text{BdG}} = 1$ characterizes a second-order TSC with Majorana corner modes. Explicitly, ν_2^{BdG} can be decomposed as

$$\begin{aligned} \nu_2^{\text{BdG}} = & \sum_{\mathbf{K} \in \text{TRIM}} \left[\frac{n_-^u(\mathbf{K})}{2} \right]_{\text{floor}} + \sum_{\mathbf{K} \in \text{TRIM}} n_-^o(\mathbf{K}) \\ & + \sum_{\mathbf{K} \in \text{TRIM}} \left[\frac{n_-^o(\mathbf{K})}{2} \right]_{\text{floor}} + \sum_{\mathbf{K} \in \text{TRIM}} \delta_2(\mathbf{K}) \mod 2, \end{aligned} \quad (5)$$

where $\delta_2(\mathbf{K}) = [n_-^u(\mathbf{K}) + 1]n_-^o(\mathbf{K}) \mod 2$. The detailed derivation is in the Supplemental Material [33]. In Eq. (5), the first term counts the parity of the number of “double Fermi surfaces”, that is, two electron-like (or hole-like) Fermi surfaces enclosing the same TRIM, in the normal state. The second term is ν_1 for the occupied bands in the normal state and the third term is ν_2 when all bands are occupied in the normal state. Finally, the last term counts the number of TRIM with an even number of unoccupied state and an odd number of negative-parity eigenstates. Figures 1(a-d) show four different normal state band structures leading to $\nu_2^{\text{BdG}} = 1$ in the weak-pairing limit, which arise from the nontrivial value of the first, second, third, and fourth terms in Eq. (5), respectively.

The analysis of Eq. (5) becomes much simpler in systems with an inversion-symmetric unit cell, where all atoms in a unit cell can be adiabatically shifted to its center without breaking inversion symmetry. In this case, the third term in Eq. (5) vanishes because an inversion-symmetric unit cell gives a topologically trivial state with $\nu_2 = 1$ when all bands are occupied. Similarly, the zero Berry phase of the whole bands makes the fourth term vanish (See Supplemental Material [33]).

Then, there remain two different channels leading to $\nu_2^{\text{BdG}} = 1$: One is odd-parity pairing in a metal with double Fermi surfaces, and the other is odd-parity pairing in a doped DSM, whose nontrivial band topology arises from the first and second terms in Eq. (5), respectively. In general, the former induces nodal superconductivity rather than a fully gapped TSC. This is because each of the two Fermi surfaces encloses a TRIM so that an odd-parity pairing function accompanies the sign reversal at two points on the Fermi surface, generating Dirac nodes. A strong pairing is required to

get a fully gapped superconducting state via pair annihilations of Dirac nodes, unless the system is fine-tuned so that the two Fermi surfaces are very close to each other. On the other hand, even weak pairing generates a fully gapped superconducting state in doped DSMs because two disconnected Fermi surfaces, each centered at a generic momentum, are paired in this case.

Higher-order TSCs in 3D and further generalization.— In 3D, $\nu_1 = 1$ indicates an odd number of nodal lines [34], and $\nu_2 = 1$ indicates an odd number of pairs of monopole nodal lines in the Brillouin zone [2, 38]. Similarly, $\nu_1^{\text{BdG}} = 1$ ($\nu_2^{\text{BdG}} = 1$) indicates a superconductor with an odd number of nodal lines (monopole nodal line pairs). In particular, the superconductor with a monopole nodal line pair exhibits the second-order topological property and carries anomalous hinge Majorana states, as in the case of chiral-symmetric monopole NLSMs [36]. Similar to 2D cases, the most promising way to get $\nu_2^{\text{BdG}} = 1$ is the process with a nontrivial second term in Eq. (5), which corresponds to doping spin-polarized NLSMs. The third term in Eq. (5) always vanishes when the whole bands are fully considered. Also the fourth term vanishes if we take an inversion-symmetric unit cell as in 2D. In the case of the first term, it may be relevant in a strong pairing limit. A double Fermi surface normally generates a superconducting state with nodal lines carrying trivial monopole charges from each Fermi surface. When the pairing amplitude is sufficiently strong, however, the two trivial nodal lines may recombine and turn into two monopole nodal lines. We note that the same mechanism corresponding to the second term in Eq. (5) was also proposed in Ref. [1] for systems with $SU(2)$ spin rotation symmetry.

The above formulation can be generalized further to $\nu_{2^n}^{\text{BdG}}$ with an arbitrary n :

$$\begin{aligned} \nu_{2^n}^{\text{BdG}} = & \sum_{\mathbf{K} \in \text{TRIM}} \left[\frac{n_-^u(\mathbf{K})}{2^n} \right]_{\text{floor}} + \sum_{\mathbf{K} \in \text{TRIM}} \left[\frac{n_-^o(\mathbf{K})}{2^{n-1}} \right]_{\text{floor}} \\ & + \sum_{\mathbf{K} \in \text{TRIM}} \left[\frac{n_-^o(\mathbf{K})}{2^n} \right]_{\text{floor}} + \sum_{\mathbf{K} \in \text{TRIM}} \delta_{2^n}(\mathbf{K}) \mod 2, \end{aligned} \quad (6)$$

where the definition of $\delta_{2^n}(\mathbf{K})$ is given in the Supplemental Material [33]. In particular, $\nu_4^{\text{BdG}} = 1$ characterizes the third-order TSC in 3D [35]. By the same reason discussed above, one can show that the best way to get a fully gapped superconductivity with $\nu_4^{\text{BdG}} = 1$ is to use the process related with the second term in Eq. (6), which can be achieved by doping a monopole NLSM (see the Supplemental Material for details [33]). To sum up, in ferromagnetic systems with an inversion-symmetric unit cell, doped nodal semimetals are the best normal state to get a higher-order TSC in the weak-pairing limit.

Lattice model.— We demonstrate our theory by using simple tight-binding models defined on rectangular or orthorhombic lattices. We construct three models in which the spin-polarized normal states are a 2D DSM, a 3D NLSM, and a 3D monopole NLSM, respectively. When an odd-parity superconducting pairing is introduced, we show that the three nodal semimetals turn into a 2D second-order TSC, a 3D monopole

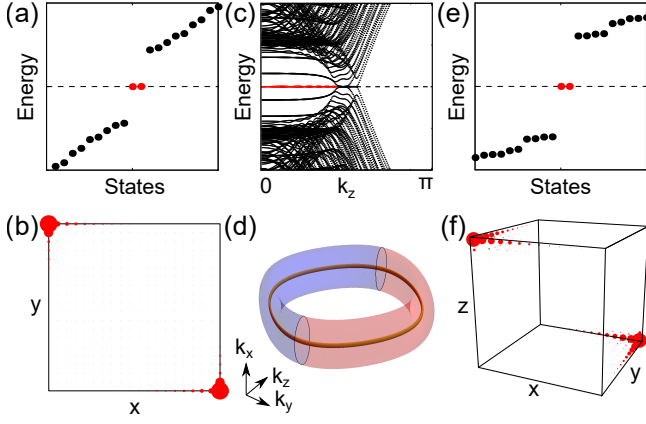


FIG. 2. Higher-order topological superconductivity from lattice models. (a,b) 2D second-order TSC obtained by adding an odd-parity pairing function to the doped 2D DSM described in Eq. (7). (a) Energy spectrum on a finite-size lattice. (b) Probability density of a Majorana zero mode (c,d) Monopole nodal line superconductor derived from a doped 3D NLSM. (c) Energy spectrum of the system, finite-sized along x and y directions. (d) Nodal structure in the Brillouin zone. The torus indicates the Fermi surface enclosing a nodal line (thick gold line) in the normal state. The blue (red) color indicates the region where the pairing function has positive (negative) sign. Two monopole nodal loops appear at the intersection, where the pairing function changes its sign. (e,f) 3D third-order TSC derived from a doped 3D monopole NLSM (e) Energy spectrum on a finite-size lattice. (f) Probability density of a Majorana zero mode

nodal line superconductor, and a 3D third-order TSC, respectively.

First, a 2D DSM can be described by the nearest-neighbor tight-binding Hamiltonian for s and p_x orbitals as

$$h = -\mu + 2t \sin k_x \sigma_y + (M - 2t \cos k_x - 2t \cos k_y) \sigma_z, \quad (7)$$

where the Pauli matrices $\sigma_{y,z}$ describe the orbital degrees of freedom with $\uparrow(\downarrow)$ indicating a $s(p_x)$ orbital. The corresponding band structure exhibits two Dirac points on the $k_x = 0$ line when $0 < M/t < 4$ at the energy $E = -\mu$. To induce superconductivity, we consider the following interaction term $H_{\text{int}} = -U \sum_{i,\sigma \neq \sigma'} n_{i,\sigma} n_{i,\sigma'} - V \sum_{\langle i,j \rangle, \sigma} n_{i,\sigma} n_{j,\sigma}$ where U (V) indicates the on-site interorbital (nearest-neighbor intraorbital) interaction, which is to be treated by mean-field approximation. The resulting odd-parity pairing leads to a fully gapped TSC whose second order band topology is clearly demonstrated in Fig. 1(a,b). Vertically stacking the 2D DSM and introducing interlayer hopping, described by $-2t \cos k_z \sigma_z$, we obtain the Hamiltonian for a 3D NLSM. Also, by further adding p_y and d_{xy} orbitals at each lattice site and introducing nearest-neighbor hopping, we obtain a 3D monopole NLSM. Adding an odd-parity pairing function in these NLSMs leads to a 3D monopole nodal line superconductor and a 3D third-order TSC whose topological properties are demonstrated in Fig. 1(c-f). Detailed information about the tight-binding models is given in the Supplemental Material [33].

Discussions.— We first discuss the effect of the inversion

asymmetry of the unit cell. For instance, in the Kagome lattice, the unit cell always breaks inversion symmetry if all atoms are required to be strictly within the unit cell. One may choose a unit cell, invariant under inversion up to lattice translations, only when the atoms in a unit cell are located on its boundary. In this case, $\nu_2 = 1$ when each atom is occupied by one electron, so the third term in Eq. (5) is nontrivial [33] for a three-band tight-binding model. Then, we have $\nu_2^{\text{BdG}} = 0$ even when the normal state is a doped DSM. However, this does not mean that MZMs is absent on the boundary. In fact, one can show that MZMs exist (do not exist) when $\nu_2^{\text{BdG}} = 0$ ($\nu_2^{\text{BdG}} = 1$) in contrast to systems having an inversion-symmetric unit cell. To obtain more conventional bulk-boundary correspondence where $\nu_2^{\text{BdG}} = 1$ always indicates the existence of MZMs independent of symmetry of the unit cell, one may define a reference trivial phase of the TSC as the limit $\mu \rightarrow -\infty$ where all electrons are unoccupied in the normal state as proposed in [58]. This gives a well-defined trivial phase for TSCs because Majorana fermions are confined to form electrons in such a limit: $|\mu|$ serves as the binding energy for Majorana fermions because $\mu c_x^\dagger c_x = 2i\mu\gamma_{1x}\gamma_{2x}$ at each site x [39], where Majorana operators $\gamma_{1,2}$ are defined from the electron annihilation operator $c_x = \gamma_{1x} + i\gamma_{2x}$.

Next, let us discuss the effect of spin-orbit coupling. When spin-orbit coupling is included, T symmetry is broken because the electron's spin cannot rotate freely independent of the orbital degrees of freedom. Since the protection of the nodal structures in both normal and superconducting states requires the combination of time reversal and inversion symmetries, the nodal structures become unstable when spin-orbit coupling exists. However, our formula in Eq. (6) is still applicable as long as inversion symmetry is preserved. Accordingly, a gapped higher-order TSC can still survive if the parity configuration does not change due to spin orbit coupling, since their topology can be protected by inversion symmetry only. In the case of the monopole nodal line superconductor, the nodes are fully gapped when T symmetry is broken due to spin-orbit coupling. The resulting gapped superconductor is a second-order TSC hosting chiral hinge states [2, 9, 40]. In fact, in the normal state, NLSM transforms to a Weyl semimetal by spin-orbit coupling as long as the parity configuration does not change. This means that, when spin-orbit coupling exists, what we observe is the transition from a Weyl semimetal to a fully gapped second-order TSC.

There exist many candidate materials for ferromagnetic spin-polarized 2D Dirac semimetals and some 3D nodal line semimetals [41–46]. One way to realize spin-triplet pairing in 2D ferromagnetic nodal semimetals is to use a superconductor-ferromagnet-superconductor heterostructure with inversion symmetry. Here, we can use conventional spin-singlet s -wave superconductors and a ferromagnet with in-plane magnetization. After spin-singlet Cooper pairs penetrate into the ferromagnet, they can turn into spin-triplet Cooper pairs because of the spin polarization in the ferromagnet [47]. In 3D, on the other hand, an intrinsic superconducting pairing is required because the proximity effect is not effective. In fact, there are several materials where the coex-

istence of ferromagnetism and superconductivity is reported including, uranium-based materials UGe_2 , URhGe , UCoGe , UTe_2 [48–54], and the more recently proposed twisted double bilayer graphene [55–57]. We hope that our work stimulates the research on higher-order TSC in ferromagnets. This will open a new route to Majorana quantum computations, where ferromagnetic nodal semimetals with spin-polarized band crossing serve as platforms for higher-order TSCs.

Finally, let us briefly comment on the extension of our result to other symmetry classes. We note that our parity formula Eq. (4) is generally applicable to any odd-parity superconductors, while we focus on ferromagnetic systems with effective time reversal symmetry since odd-parity pairing is natural in these systems. Furthermore, we expect that nodal semimetals required by eigenvalues of symmetry operator G can lead to a G -protected d th-order TSCs, which can be shown by extending Eq. (4) to eigenvalues of G , as is outlined in [29] for k th-order TSCs with $k < d$. We leave more detailed theoretical analysis for future work.

ACKNOWLEDGMENTS

We are grateful to A. Skurativska, T. Neupert, and M. H. Fischer for sharing a related manuscript [58]. We thank Seunghun Lee, Yoonseok Hwang, Taekoo Oh, and Se Young Park for helpful discussions. J.A. was supported by IBS-R009-D1. B.-J.Y. was supported by the Institute for Basic Science in Korea (Grant No. IBS-R009-D1) and Basic Science Research Program through the National Research Foundation of Korea (NRF) (Grant No. 0426-20190008), and the POSCO Science Fellowship of POSCO TJ Park Foundation (No. 0426-20180002). This work was supported in part by the U.S. Army Research Office under Grant Number W911NF-18-1-0137.

Note added.— Recently, we became aware of two related manuscripts [58, 59]. Reference [59] also suggests that a third-order topological superconductivity can be obtained by odd-parity pairing in a doped nodal line semimetal. In Ref. [58], the authors also have related the higher-order topology of inversion-symmetric superconductors to the parity of the normal state.

-
- [1] M. Sato and Y. Ando, “Topological superconductors: a review,” *Rep. Prog. Phys.* **80**, 076501 (2017).
 - [2] J. Alicea, “New directions in the pursuit of Majorana fermions in solid state systems,” *Rep. Prog. Phys.* **75**, 076501 (2012).
 - [3] S. Das Sarma, M. Freedman, and C. Nayak, “Majorana zero modes and topological quantum computation,” *npj Quantum Inf.* **1**, 15001 (2015).
 - [4] A. Kitaev, “Fault-tolerant quantum computation by anyons,” *Ann. Phys.* **303**, 2–30 (2003).
 - [5] C. Nayak, S. H. Simon, A. Stern, M. Freedman, and S. Das Sarma, “Non-abelian anyons and topological quantum computation,” *Rev. Mod. Phys.* **80**, 1083 (2008).
 - [6] L. Fu and E. Berg, “Odd-parity topological superconductors: theory and application to $\text{Cu}_x\text{Bi}_2\text{Se}_3$,” *Phys. Rev. Lett.* **105**, 097001 (2010).
 - [7] M. Sato, “Topological properties of spin-triplet superconductors and Fermi surface topology in the normal state,” *Phys. Rev. B* **79**, 214526 (2009).
 - [8] M. Sato, “Topological odd-parity superconductors,” *Phys. Rev. B* **81**, 220504(R) (2010).
 - [9] E. Khalaf, “Higher-order topological insulators and superconductors protected by inversion symmetry,” *Phys. Rev. B* **97**, 205136 (2018).
 - [10] Y. You, D. Litinski, and F. von Oppen, “Higher order topological superconductors as generators of quantum codes,” *Phys. Rev. B* **100**, 054513 (2019).
 - [11] M. Geier, L. Trifunovic, M. Hoskam, and P. W. Brouwer, “Second-order topological insulators and superconductors with an order-two crystalline symmetry,” *Phys. Rev. B* **97**, 205135 (2018).
 - [12] L. Trifunovic and P. W. Brouwer, “Higher-order bulk-boundary correspondence for topological crystalline phases,” *Phys. Rev. X* **9**, 011012 (2019).
 - [13] Y. Wang, M. Lin, and T. L. Hughes, “Weak-pairing higher order topological superconductors,” *Phys. Rev. B* **98**, 165144 (2018).
 - [14] T. E. Pahomi, M. Sgrist, and A. A. Soluyanov, “Braiding Majorana corner modes in a two-layer second-order topological insulator,” *arXiv:1904.07822* (2019).
 - [15] T. Liu, J. J. He, F. Nori, *et al.*, “Majorana corner states in a two-dimensional magnetic topological insulator on a high-temperature superconductor,” *Phys. Rev. B* **98**, 245413 (2018).
 - [16] Q. Wang, C.-C. Liu, Y.-M. Lu, and F. Zhang, “High-temperature Majorana corner states,” *Phys. Rev. Lett.* **121**, 186801 (2018).
 - [17] Z. Yan, F. Song, and Z. Wang, “Majorana corner modes in a high-temperature platform,” *Phys. Rev. Lett.* **121**, 096803 (2018).
 - [18] C.-H. Hsu, P. Stano, J. Klinovaja, and D. Loss, “Majorana Kramers pairs in higher-order topological insulators,” *Phys. Rev. Lett.* **121**, 196801 (2018).
 - [19] X. Zhu, “Second-order topological superconductors with mixed pairing,” *Phys. Rev. Lett.* **122**, 236401 (2019).
 - [20] K. Laubscher, D. Loss, and J. Klinovaja, “Fractional topological superconductivity and parafermion corner states,” *Phys. Rev. Research* **1**, 032017 (2019).
 - [21] X. Zhu, “Tunable Majorana corner states in a two-dimensional second-order topological superconductor induced by magnetic fields,” *Phys. Rev. B* **97**, 205134 (2018).
 - [22] Y. Volpez, D. Loss, and J. Klinovaja, “Second-order topological superconductivity in π -junction rashba layers,” *Phys. Rev. Lett.* **122**, 126402 (2019).
 - [23] Y.-T. Hsu, W. S. Cole, R.-X. Zhang, and J. D. Sau, “Inversion-protected topological crystalline superconductivity in monolayer WTe_2 ,” *arXiv:1904.06361* (2019).
 - [24] Y.-J. Wu, J. Hou, X. Luo, Y. Li, and C. Zhang, “In-plane Zeeman field induced Majorana corner and hinge modes in an s -wave superconductor heterostructure,” *arXiv:1905.08896* (2019).
 - [25] R.-X. Zhang, W. S. Cole, X. Wu, and S. Das Sarma, “Higher order topology and nodal topological superconductivity in $\text{Fe}(\text{Se},\text{Te})$ heterostructures,” *Phys. Rev. Lett.* **123**, 167001 (2019).

- [26] Z. Wu, Z. Yan, and W. Huang, “Higher-order topological superconductivity: Possible realization in fermi gases and Sr_2RuO_4 ,” *Phys. Rev. B* **99**, 020508(R) (2019).
- [27] S. Franca, D. V. Efremov, and I. C. Fulga, “Phase tunable second-order topological superconductor,” *Phys. Rev. B* **100**, 075415 (2019).
- [28] M. Kheirkhah, Y. Nagai, C. Chen, and F. Marsiglio, “Majorana corner flat bands in two-dimensional second-order topological superconductors,” arXiv:1904.00990 (2019).
- [29] S. Ono, Y. Yanase, and H. Watanabe, “Symmetry indicators for topological superconductors,” *Phys. Rev. Research* **1**, 013012 (2019).
- [30] C. Fang and L. Fu, “New classes of three-dimensional topological crystalline insulators: Nonsymmorphic and magnetic,” *Phys. Rev. B* **91**, 161105(R) (2015).
- [2] J. Ahn, D. Kim, Y. Kim, and B.-J. Yang, “Band topology and linking structure of nodal line semimetals with Z_2 monopole charges,” *Phys. Rev. Lett.* **121**, 106403 (2018).
- [1] T. Bzdušek and M. Sigrist, “Robust doubly charged nodal lines and nodal surfaces in centrosymmetric systems,” *Phys. Rev. B* **96**, 155105 (2017).
- [33] See Supplemental Material at [URL will be inserted by publisher] for the derivation of the generalized parity formula and tight-binding models of spin-polarized higher-order superconductors.
- [34] Y. Kim, B. J. Wieder, C. L. Kane, and A. M. Rappe, “Dirac line nodes in inversion-symmetric crystals,” *Phys. Rev. Lett.* **115**, 036806 (2015).
- [35] Y. Hwang, J. Ahn, and B.-J. Yang, “Fragile topology protected by inversion symmetry: Diagnosis, bulk-boundary correspondence, and wilson loop,” *Phys. Rev. B* **100**, 205126 (2019).
- [36] Z. Wang, B. J. Wieder, J. Li, B. Yan, and B. A. Bernevig, “Higher-order topology, monopole nodal lines, and the origin of large fermi arcs in transition metal dichalcogenides XTe_2 ($\text{X} = \text{Mo}, \text{W}$),” *Phys. Rev. Lett.* **123**, 186401 (2019).
- [37] J. Ahn, S. Park, and B.-J. Yang, “Failure of Nielsen-Ninomiya theorem and fragile topology in two-dimensional systems with space-time inversion symmetry: Application to twisted bilayer graphene at magic angle,” *Phys. Rev. X* **9**, 021013 (2019).
- [38] Z. Song, T. Zhang, and C. Fang, “Diagnosis for nonmagnetic topological semimetals in the absence of spin-orbital coupling,” *Phys. Rev. X* **8**, 031069 (2018).
- [39] A. Y. Kitaev “Unpaired Majorana fermions in quantum wires,” *Phys. Usp.* **44**, 131 (2001).
- [40] E. Khalaf, H. C. Po, A. Vishwanath, and H. Watanabe, “Symmetry indicators and anomalous surface states of topological crystalline insulators,” *Phys. Rev. X* **8**, 031070 (2018).
- [41] X. Wang, T. Li, Z. Cheng, X.-L. Wang, and H. Chen, Recent advances in dirac spin-gapless semiconductors, *Appl. Phys. Rev.* **5**, 041103 (2018).
- [42] J. Zou, Z. He, and G. Xu, The study of magnetic topological semimetals by first principles calculations, *npj Comput. Mater.* **5**, 1 (2019).
- [43] R. Wang, J. Z. Zhao, Y. J. Jin, Y. P. Du, Y. X. Zhao, H. Xu, and S. Y. Tong, Nodal line fermions in magnetic oxides, *Phys. Rev. B* **97**, 241111(R) (2018).
- [44] K. Kim, J. Seo, E. Lee, K.-T. Ko, B. Kim, B. G. Jang, J. M. Ok, J. Lee, Y. J. Jo, W. Kang, *et al.*, Large anomalous hall current induced by topological nodal lines in a ferromagnetic van der waals semimetal, *Nat. Mater.* **17**, 794 (2018).
- [45] C. Chen, Z.-M. Yu, S. Li, Z. Chen, X.-L. Sheng, and S. A. Yang, Weyl-loop half-metal in $\text{Li}_3(\text{FeO}_3)_2$, *Phys. Rev. B* **99**, 075131 (2019).
- [46] X. Zuo, A. C. Dias, F. Liu, L. Han, H. Li, Q. Gao, X. Jiang, D. Li, B. Cui, D. Liu, F. Qu, Fully spin-polarized open and closed nodal lines in β -borophene by magnetic proximity effect, *Phys. Rev. B* **100**, 115423 (2019).
- [47] M. Eschrig, J. Kopu, J. C. Cuevas, and G. Schön, “Theory of half-metal/superconductor heterostructures,” *Phys. Rev. Lett.* **90**, 137003 (2003).
- [48] D. Aoki, K. Ishida, and J. Flouquet, “Review of U-based ferromagnetic superconductors: Comparison between UGe_2 , URhGe , and UCoGe ,” *J. Phys. Soc. Jpn.* **88**, 022001 (2019).
- [49] S. S. Saxena, P. Agarwal, K. Ahilan, F. M. Grosche, R. K. W. Haselwimmer, M. J. Steiner, E. Pugh, I. R. Walker, S. R. Julian, P. Monthoux, *et al.*, “Superconductivity on the border of itinerant-electron ferromagnetism in UGe_2 ,” *Nature (London)* **406**, 587 (2000).
- [50] A. Huxley, I. Sheikin, E. Ressouche, N. Kernavanois, D. Braithwaite, R. Calemczuk, and J. Flouquet, “ UGe_2 : A ferromagnetic spin-triplet superconductor,” *Phys. Rev. B* **63**, 144519 (2001).
- [51] D. Aoki, A. Huxley, E. Ressouche, D. Braithwaite, J. Flouquet, Jean-Pascal Brison, Elsa Lhotel, and Carley Paulsen, “Coexistence of superconductivity and ferromagnetism in URhGe ,” *Nature (London)* **413**, 613 (2001).
- [52] N. T. Huy, A. Gasparini, D. E. De Nijs, Y. Huang, J. C. P. Klaasse, T. Gortenmulder, A. de Visser, A. Hamann, T. Görlach, and H. v. Löhneysen, “Superconductivity on the border of weak itinerant ferromagnetism in UCoGe ,” *Phys. Rev. Lett.* **99**, 067006 (2007).
- [53] A. D. Huxley, “Ferromagnetic superconductors,” *Physica C* **514**, 368–377 (2015).
- [54] S. Ran, C. Eckberg, Q.-P. Ding, Y. Furukawa, T. Metz, S. R. Saha, I.-L. Liu, M. Zic, H. Kim, J. Paglione, *et al.*, Nearly ferromagnetic spin-triplet superconductivity, *Science* **365**, 684 (2019).
- [55] X. Liu, Z. Hao, E. Khalaf, J. Y. Lee, K. Watanabe, T. Taniguchi, A. Vishwanath, and P. Kim, “Spin-polarized correlated insulator and superconductor in twisted double bilayer graphene,” arXiv:1903.08130 (2019).
- [56] J. Y. Lee, E. Khalaf, S. Liu, X. Liu, Z. Hao, P. Kim, and A. Vishwanath, “Theory of correlated insulating behaviour and spin-triplet superconductivity in twisted double bilayer graphene,” *Nat. Commun.* **10**, 5333 (2019).
- [57] C. Shen, N. Li, S. Wang, Y. Zhao, J. Tang, J. Liu, J. Tian, Y. Chu, K. Watanabe, T. Taniguchi, *et al.*, “Observation of superconductivity with t_c onset at 12K in electrically tunable twisted double bilayer graphene,” arXiv:1903.06952 (2019).
- [58] A. Skurativska, T. Neupert, and M. H. Fischer, “Atomic limit and inversion-symmetry indicators for topological superconductors,” *Phys. Rev. Research* **2**, 013064 (2020).
- [59] Z. Yan, “Higher-order topological odd-parity superconductors,” *Phys. Rev. Lett.* **123**, 177001 (2019).

Supplemental Material for “Higher-order topological ferromagnetic superconductivity”

Junyeong Ahn^{1,2,3} and Bohm-Jung Yang^{1,2,3,*}

¹*Center for Correlated Electron Systems, Institute for Basic Science (IBS), Seoul 08826, Korea*

²*Department of Physics and Astronomy, Seoul National University, Seoul 08826, Korea*

³*Center for Theoretical Physics (CTP), Seoul National University, Seoul 08826, Korea*

CONTENTS

Acknowledgments	5
References	5
I. Odd-Parity Pairing in the Weak Pairing Limit in View of Symmetry and Topology	1
II. Parity Eigenvalues and Odd-Parity Pairing	2
A. Parity indices of odd-parity superconductors.	2
B. Third-order topological superconductor in three dimensions.	3
III. General Form of Model Hamiltonians	4
A. Two-band normal state and odd-parity pairing	4
B. Four-band normal state and odd-parity pairing	5
C. Three-band normal state and odd-parity pairing	6
IV. Tight-Binding Models	7
A. Dirac semimetal and second-order topological superconductor in two dimensions	7
B. Nodal line semimetal and second-order topological nodal superconductor in three dimensions	8
C. Monopole nodal line semimetal and third-order topological superconductor in three dimensions	9
V. More on Tight-Binding Models in Two Dimensions	10
A. Hexagonal lattice	10
1. Normal state	10
2. Superconducting state	10
B. Kagome lattice	11
1. Normal state	11
2. Superconducting state	12
References	13

I. ODD-PARITY PAIRING IN THE WEAK PAIRING LIMIT IN VIEW OF SYMMETRY AND TOPOLOGY

Spin-polarized electrons in centrosymmetric systems form odd-parity pairing in the weak pairing limit, which can be understood from the Fermi statistics of electrons. This can be alternatively explained from the viewpoint of topological charges of band crossing nodes. Let us note that a nondegenerate Fermi surface in the normal state is described as a two-fold degenerate $(d - 1)$ -dimensional node in d dimensions in the Bogoliubov-de Gennes (BdG) formulation in the absence of superconducting pairing. Table I shows that a zero-dimensional Z_2 topological charge exists in the superconducting phase (does not exist) for an even-parity (odd-parity) pairing, regardless of whether there exists effective time reversal symmetry under T satisfying $T^2 = 1$. If we consider even-parity pairing, the zero-dimensional Z_2 topological charge serves as the topological charge of the $(d - 1)$ -dimensional node. Therefore, any weak even-parity superconducting pairing preserves the $(d - 1)$ -dimensional node in the BdG Hamiltonian. To open the gap, two Fermi surfaces should meet to cancel the topological charge, and this process requires a strong superconducting pairing. In contrast, weak odd-parity pairing opens the gap on the Fermi surface because $(d - 1)$ -dimensional node is not protected in the BdG formulation. Accordingly, an odd-parity pairing state is energetically favorable than an even-parity pairing state.

II. PARITY EIGENVALUES AND ODD-PARITY PAIRING

A. Parity indices of odd-parity superconductors.

In the main text, we define parity indices ν_{2^n} that counts the number of 2^n band inversion occurring at each time-reversal-invariant momentum (TRIM):

$$\nu_{2^n} = \sum_{\mathbf{K} \in \text{TRIM}} \left[\frac{n_-^o(\mathbf{K})}{2^n} \right]_{\text{floor}}, \quad (1)$$

where we define $n_{\pm}^{o(u)}(\mathbf{K})$ as the number of occupied (unoccupied) states at \mathbf{K} with inversion parity ± 1 . One of our main result is the decomposition of the parity indices for the odd-parity BdG Hamiltonian into

$$\nu_{2^n}^{\text{BdG}} = \sum_{\mathbf{K} \in \text{TRIM}} \left[\frac{n_+^u(\mathbf{K})}{2^n} \right]_{\text{floor}} + \sum_{\mathbf{K} \in \text{TRIM}} \left[\frac{n_-^o(\mathbf{K})}{2^{n-1}} \right]_{\text{floor}} + \sum_{\mathbf{K} \in \text{TRIM}} \left[\frac{n_-^u(\mathbf{K})}{2^n} \right]_{\text{floor}} + \sum_{\mathbf{K} \in \text{TRIM}} \delta_{2^n}(\mathbf{K}) \quad (2)$$

modulo two, where $n^u(\mathbf{K}) = n_+^u(\mathbf{K}) + n_-^u(\mathbf{K})$, $n_-(\mathbf{K}) = n_-^o(\mathbf{K}) + n_-^u(\mathbf{K})$, and $\delta_{2^n}(\mathbf{K})$ is defined below. Here, we derive the decomposition Eq. (2) as follows:

$$\begin{aligned} \nu_{2^n}^{\text{BdG}} &= \sum_{\mathbf{K} \in \text{TRIM}} \left[\frac{n_-^{\text{o,BdG}}(\mathbf{K})}{2^n} \right]_{\text{floor}} \\ &= \sum_{\mathbf{K} \in \text{TRIM}} \left[\frac{n_+^u(\mathbf{K}) + n_-^o(\mathbf{K})}{2^n} \right]_{\text{floor}} \\ &= \sum_{\mathbf{K} \in \text{TRIM}} \left[\frac{n_+^u(\mathbf{K}) + n_-^u(\mathbf{K}) + 2n_-^o(\mathbf{K}) - n_-^o(\mathbf{K}) - n_-^u(\mathbf{K})}{2^n} \right]_{\text{floor}} \\ &= \sum_{\mathbf{K} \in \text{TRIM}} \left[\frac{n_+^u(\mathbf{K})}{2^n} + \frac{n_-^o(\mathbf{K})}{2^{n-1}} - \frac{n_-^u(\mathbf{K})}{2^n} \right]_{\text{floor}} \\ &= \sum_{\mathbf{K} \in \text{TRIM}} \left(\left[\frac{n_+^u(\mathbf{K})}{2^n} \right]_{\text{floor}} + \left[\frac{n_-^o(\mathbf{K})}{2^{n-1}} \right]_{\text{floor}} - \left[\frac{n_-^u(\mathbf{K})}{2^n} \right]_{\text{floor}} + \delta_{2^n}(\mathbf{K}) \right) \\ &= \sum_{\mathbf{K} \in \text{TRIM}} \left[\frac{n_+^u(\mathbf{K})}{2^n} \right]_{\text{floor}} + \sum_{\mathbf{K} \in \text{TRIM}} \left[\frac{n_-^o(\mathbf{K})}{2^{n-1}} \right]_{\text{floor}} + \sum_{\mathbf{K} \in \text{TRIM}} \left[\frac{n_-^u(\mathbf{K})}{2^n} \right]_{\text{floor}} + \sum_{\mathbf{K} \in \text{TRIM}} \delta_{2^n}(\mathbf{K}) \end{aligned} \quad (3)$$

modulo two, where $\delta_{2^n}(\mathbf{K})$ is defined by the fourth and fifth lines, and we flip the sign of the third term in the last line, which is possible because we count only mod 2.

TABLE I. Classification of topological charges of nodes in spin-polarized centrosymmetric normal and superconducting states. We adopt the notation proposed by Bzdusek-Sigrist [1] to indicate the nodal class. Here, P , T , C , and S are spatial inversion, time reversal, particle-hole, and chiral symmetry operators. Since P , T , and C all reverse the sign of the crystal momentum, PT , PC , and S do not change the crystal momentum. These are relevant for the protection of band degeneracies appearing at generic low-symmetry momenta in the Brillouin zone. “0” in the entry means the absence of symmetry in the third-fifth column and means the absence of topologically nontrivial phase in the sixth-ninth column. δ is the dimension of the submanifold enclosing a node in the Brillouin zone, on which the topological charge is defined. The name in the parenthesis after \mathbb{Z} or \mathbb{Z}_2 indicates the relevant topological invariant.

Pairing-parity	Nodal class	$(PT)^2$	$(PC)^2$	S^2	$\delta = 0$	$\delta = 1$	$\delta = 2$
Normal state	$A+\mathcal{I}$	0	0	0	0	0	\mathbb{Z} (Chern number)
Even	$D+\mathcal{I}$	0	1	0	\mathbb{Z}_2 (Pfaffian)	0	$2\mathbb{Z}$ (Chern number)
Odd	$C+\mathcal{I}$	0	-1	0	0	0	\mathbb{Z} (Chern number)
Normal state	$AI+\mathcal{I}$	1	0	0	0	\mathbb{Z}_2 (Berry phase)	\mathbb{Z}_2 (Stiefel-Whitney number)
Even	$BDI+\mathcal{I}$	1	1	1	\mathbb{Z}_2 (Pfaffian)	\mathbb{Z}_2 (winding number)	0
Odd	$CI+\mathcal{I}$	1	-1	1	0	\mathbb{Z} (winding number)	\mathbb{Z}_2 (Stiefel-Whitney number)

B. Third-order topological superconductor in three dimensions.

We assume time reversal T and inversion P symmetries that satisfy $T^2 = P^2 = 1$ in the normal state, and an additional particle-hole C symmetry that satisfies $C^2 = 1$ and $CP = -PC$ in the superconducting state. Accordingly, in both normal and superconducting states, nodal points and nodal lines are stable in two and three dimensions, respectively. In the main text, we show that, when we can take an inversion-invariant unit cell, the normal state need to obtain a weak-pairing odd-parity second-order topological superconductor with $\nu_2^{\text{BdG}} = 1$ in two and three dimensions is a semimetal characterized by $\nu_1 = 1$. Here, we show that, when we can take a unit cell that is inversion-invariant, we need a monopole nodal line semimetal characterized by $\nu_2 = 1$ as a normal state to achieve a fully gapped third-order topological superconductor with $\nu_4^{\text{BdG}} = 1$ in three dimensions by weak odd-parity pairing. To prove this statement, we use the following three conditions:

1. there is no Fermi surface enclosing a TRIM,
2. the superconducting state has no nodes requires by inversion parity, and
3. the unit cell is inversion-invariant.

Note that the first and second conditions required to get a fully gapped superconductor. The first condition is required to obtain a fully gapped superconducting state in the weak pairing limit, because a weak odd-parity pairing creates nodes on each Fermi surface enclosing a TRIM due to the sign change of the pairing function on the Fermi surface. The second condition states that there is no parity-enforced node in the superconducting state.

We first write $n^u(\mathbf{K})$, $n_-^o(\mathbf{K})$, and $n_-(\mathbf{K})$ in binary.

$$\begin{aligned} n^u(\mathbf{K}) &= \alpha_1(\mathbf{K}) + 2\alpha_2(\mathbf{K}) + 4\alpha_4(\mathbf{K}) + \dots, \\ n_-^o(\mathbf{K}) &= \beta_1(\mathbf{K}) + 2\beta_2(\mathbf{K}) + 4\beta_4(\mathbf{K}) + \dots, \\ n_-(\mathbf{K}) &= \gamma_1(\mathbf{K}) + 2\gamma_2(\mathbf{K}) + 4\gamma_4(\mathbf{K}) + \dots, \end{aligned} \quad (4)$$

where $\alpha_{2^n}(\mathbf{K})$, $\beta_{2^n}(\mathbf{K})$, and $\gamma_{2^n}(\mathbf{K})$ are 0 or 1 for all nonnegative integer n . Then,

$$\begin{aligned} \nu_{2^n} &= \sum_{\mathbf{K} \in \text{TRIM}} \beta_{2^n}(\mathbf{K}) \mod 2, \\ \nu_{2^n}^{\text{BdG}} &= \sum_{\mathbf{K} \in \text{TRIM}} \alpha_{2^n}(\mathbf{K}) + \sum_{\mathbf{K} \in \text{TRIM}} \beta_{2^{n-1}}(\mathbf{K}) + \sum_{\mathbf{K} \in \text{TRIM}} \gamma_{2^n}(\mathbf{K}) + \sum_{\mathbf{K} \in \text{TRIM}} \delta_{2^n}(\mathbf{K}) \mod 2, \end{aligned} \quad (5)$$

The condition 1 and 3 requires all $\alpha_{2^n}(\mathbf{K})$ s and all $\gamma_{2^n}(\mathbf{K})$ s to be constants (independent of \mathbf{K}), respectively, i.e.,

$$\begin{aligned} \alpha_{2^n}(\mathbf{K}) &= \alpha_{2^n} \quad \forall n, \mathbf{K}, \\ \gamma_{2^n}(\mathbf{K}) &= \gamma_{2^n} \quad \forall n, \mathbf{K}. \end{aligned} \quad (6)$$

Here, $\gamma_{2^n}(\mathbf{K})$ s are constants because, in the case when we can take an inversion-invariant unit cell, all electronic states can be continuously deformed to the unit cell center, such that $n_-(\mathbf{K})$ is independent of \mathbf{K} . The condition 2 requires that the superconducting state does not have symmetry-required nodes, i.e., $\nu_1^{\text{BdG}} = \nu_2^{\text{BdG}} = 0$ because ν_1^{BdG} on a plane counts the number of nodal lines penetrating the plane (2D sub-Brillouin zone), and ν_2^{BdG} counts the number of monopole nodal line pairs in the Brillouin zone:

$$\begin{aligned} \nu_1^{\text{BdG}} &= \sum_{\substack{\mathbf{K} \in \text{TRIM} \\ \text{in a plane}}} \alpha_1(\mathbf{K}) = 0 \mod 2 \\ \nu_2^{\text{BdG}} &= \sum_{\mathbf{K} \in \text{TRIM}} [\alpha_2(\mathbf{K}) + \beta_1(\mathbf{K}) + \gamma_2(\mathbf{K}) + \delta_2(\mathbf{K})] = \sum_{\mathbf{K} \in \text{TRIM}} \beta_1(\mathbf{K}) = 0 \mod 2, \end{aligned} \quad (7)$$

where, in the second line, we use $\sum_{\mathbf{K} \in \text{TRIM}} \alpha_2(\mathbf{K}) = 0 \mod 2$, $\sum_{\mathbf{K} \in \text{TRIM}} \gamma_2(\mathbf{K}) = 0 \mod 2$, and $\sum_{\mathbf{K} \in \text{TRIM}} \delta_2(\mathbf{K}) = 0 \mod 2$ because $\delta_2(\mathbf{K}) = [\alpha_1(\mathbf{K})/2 - \gamma_1(\mathbf{K})/2]_{\text{floor}}$ is either $\alpha_1(\mathbf{K})$ or $1 - \alpha_1(\mathbf{K})$ depending on the value of the constant $\gamma_1(\mathbf{K}) = \gamma_1$. While the first line is redundant as it can also be derived from the condition 1, the second line gives a new constraint on $\beta_1(\mathbf{K})$.

It immediately follows that

$$\begin{aligned} \sum_{\mathbf{K} \in \text{TRIM}} \alpha_4(\mathbf{K}) &= \alpha_4 \sum_{\mathbf{K} \in \text{TRIM}} 1 = 0 \mod 2, \\ \sum_{\mathbf{K} \in \text{TRIM}} \gamma_4(\mathbf{K}) &= \gamma_4 \sum_{\mathbf{K} \in \text{TRIM}} 1 = 0 \mod 2. \end{aligned} \quad (8)$$

Also, we have

$$\sum_{\mathbf{K} \in \text{TRIM}} \delta_4(\mathbf{K}) = \sum_{\mathbf{K} \in \text{TRIM}} \left[\frac{1}{4}\alpha_1 + \frac{1}{2}\alpha_2 - \frac{1}{4}\gamma_1 - \frac{1}{2}\gamma_2 + \frac{1}{2}\beta_1(\mathbf{K}) \right]_{\text{floor}} = 0 \pmod{2}. \quad (9)$$

This can be shown as follows. First, note that $\delta_4(\mathbf{K}) = [\alpha_1/4 + \alpha_2/2 - \gamma_1/4 - \gamma_2/2 + \beta_1(\mathbf{K})/2]_{\text{floor}}$ is either independent of $\beta_1(\mathbf{K})$ or dependent on the value of $\beta_1(\mathbf{K})$. In the former, since $\delta_4(\mathbf{K})$ is an integer that is independent of \mathbf{K} , Eq. (9) is obviously valid. In the latter, $\delta_4(\mathbf{K})$ can be either $\beta_1(\mathbf{K}) \pmod{2}$ or $1 - \beta_1(\mathbf{K}) \pmod{2}$, so $\sum_{\mathbf{K}} \delta_4(\mathbf{K}) = 0 \pmod{2}$ is guaranteed by the second line in Eq. (7). Thus, we have Eq. (9).

In conclusion, $\nu_4^{\text{BdG}} = 1$ only when the normal state is a monopole nodal line semimetal characterized by $\nu_2 = 1$ when the three conditions stated in the beginning of this subsection are satisfied, because then

$$\begin{aligned} \nu_4^{\text{BdG}} &= \sum_{\mathbf{K} \in \text{TRIM}} \alpha_4(\mathbf{K}) + \sum_{\mathbf{K} \in \text{TRIM}} \beta_2(\mathbf{K}) + \sum_{\mathbf{K} \in \text{TRIM}} \gamma_4(\mathbf{K}) + \sum_{\mathbf{K} \in \text{TRIM}} \delta_4(\mathbf{K}) \pmod{2} \\ &= \sum_{\mathbf{K} \in \text{TRIM}} \beta_2(\mathbf{K}) \pmod{2} \\ &= \sum_{\mathbf{K} \in \text{TRIM}} \left[\frac{n_-^o(\mathbf{K})}{2} \right]_{\text{floor}} \pmod{2} \\ &= \nu_2 \pmod{2}. \end{aligned} \quad (10)$$

III. GENERAL FORM OF MODEL HAMILTONIANS

Here we write down the most general form of the two-, three-, and four-band normal state Hamiltonians with inversion P and time reversal T symmetries with $P^2 = T^2$ and their odd-parity BdG Hamiltonians whose particle-hole operator C satisfies $C^2 = 1$. The two- and four-band normal state models are used in In Sec. IV, and the three-band normal state Hamiltonian is studied here for a discussion on the tight-binding model on the Kagome lattice in Sec. V. In our notations, $\sigma_{i=x,y,z}$ and $\rho_{i=x,y,z}$ are Pauli matrices for the orbital degrees of freedom, $\lambda_{i=0,\dots,8}$ are Gell-Mann matrices for the orbital degrees of freedom, and $\tau_{i=x,y,z}$ are Pauli matrices for the Nambu space.

A. Two-band normal state and odd-parity pairing

We take inversion P and time reversal T symmetry operators as

$$P = \sigma_z, \quad T = K. \quad (11)$$

Then, the 2×2 normal state Hamiltonian has the form of

$$h(\mathbf{k}) = -\mu(\mathbf{k}) + f_1(\mathbf{k})\sigma_y + f_2(\mathbf{k})\sigma_z, \quad (12)$$

where

$$\begin{aligned} \mu(\mathbf{k}) &= +\mu(-\mathbf{k}) \\ f_1(\mathbf{k}) &= -f_1(-\mathbf{k}), \\ f_2(\mathbf{k}) &= +f_2(-\mathbf{k}). \end{aligned} \quad (13)$$

The energy spectrum is given by

$$E(\mathbf{k}) = -\mu(\mathbf{k}) \pm \sqrt{f_1^2(\mathbf{k}) + f_2^2(\mathbf{k})}. \quad (14)$$

In the case of odd-parity pairing, inversion operator acts on the particle and hole sector with a different sign, so particle-hole C , inversion P , and time reversal T symmetry operators are

$$C = \tau_x K, \quad P = \tau_z \sigma_z, \quad T = K. \quad (15)$$

The 4×4 BdG Hamiltonian compatible with those symmetries is

$$\begin{aligned} H(\mathbf{k}) &= -\mu(\mathbf{k})\tau_z + f_1(\mathbf{k})\tau_z\sigma_y + f_2(\mathbf{k})\tau_z\sigma_z + \Delta_1(\mathbf{k})\tau_y + \Delta_2(\mathbf{k})\tau_y\sigma_y + \Delta_3(\mathbf{k})\tau_y\sigma_z \\ &= f_1(\mathbf{k})\Gamma_1 + f_2(\mathbf{k})\Gamma_2 + \Delta_1(\mathbf{k})\Gamma_3 + \Delta_2(\mathbf{k})\Gamma_{14} + \Delta_3(\mathbf{k})\Gamma_{24} + \mu(\mathbf{k})\Gamma_{34}, \end{aligned} \quad (16)$$

where

$$\begin{aligned} \Delta_{i=2}(\mathbf{k}) &= +\Delta_{i=2}(-\mathbf{k}), \\ \Delta_{i=1,3}(\mathbf{k}) &= -\Delta_{i=1,3}(-\mathbf{k}), \end{aligned} \quad (17)$$

and we define mutually anticommuting Gamma matrices by

$$\begin{aligned} \Gamma_1 &= \tau_z\sigma_y, \\ \Gamma_2 &= \tau_z\sigma_z, \\ \Gamma_3 &= \tau_y, \\ \Gamma_4 &= \tau_x, \\ \Gamma_5 &= \tau_z\sigma_x, \end{aligned} \quad (18)$$

and $\Gamma_{ij} = -i\Gamma_i\Gamma_j$. The spectrum of the BdG Hamiltonian is given by [1]

$$E(\mathbf{k}) = \pm\sqrt{\mathbf{a}^2 + \mathbf{b}^2 \pm 2|\mathbf{a} \times \mathbf{b}|}, \quad (19)$$

where

$$\begin{aligned} \mathbf{a} &= (f_1, f_2, \Delta_1,), \\ \mathbf{b} &= (\Delta_2, \Delta_3, \mu). \end{aligned} \quad (20)$$

B. Four-band normal state and odd-parity pairing

As above, we take symmetry operators as

$$P = \sigma_z, \quad T = K. \quad (21)$$

Then, the 4×4 normal state Hamiltonian has the form of

$$\begin{aligned} h(\mathbf{k}) &= -\mu(\mathbf{k}) + f_1(\mathbf{k})\rho_y\sigma_x + f_2(\mathbf{k})\sigma_y + f_3(\mathbf{k})\sigma_z \\ &\quad + m_1(\mathbf{k})\rho_z + m_2(\mathbf{k})\rho_x + m_3(\mathbf{k})\rho_x\sigma_z + m_4(\mathbf{k})\rho_z\sigma_z + m_5(\mathbf{k})\rho_x\sigma_y + m_6(\mathbf{k})\rho_z\sigma_y \\ &= -\mu(\mathbf{k}) + f_1(\mathbf{k})\gamma_1 + f_2(\mathbf{k})\gamma_2 + f_3(\mathbf{k})\gamma_3 \\ &\quad - m_1(\mathbf{k})\gamma_{14} + m_2(\mathbf{k})\gamma_{15} - m_3(\mathbf{k})\gamma_{24} - m_4(\mathbf{k})\gamma_{25} + m_5(\mathbf{k})\gamma_{34} + m_6(\mathbf{k})\gamma_{35}, \end{aligned} \quad (22)$$

where

$$\begin{aligned} \mu(\mathbf{k}) &= +\mu(-\mathbf{k}), \\ f_{i=1,2}(\mathbf{k}) &= -f_{i=1,2}(-\mathbf{k}), \\ f_3(\mathbf{k}) &= +f_3(-\mathbf{k}), \\ m_{i=1,2,3,4}(\mathbf{k}) &= +m_{i=1,2,3,4}(-\mathbf{k}), \\ m_{i=5,6}(\mathbf{k}) &= -m_{i=5,6}(-\mathbf{k}), \end{aligned} \quad (23)$$

and we define

$$\begin{aligned} \gamma_1 &= \rho_y\sigma_x, \\ \gamma_2 &= \sigma_y, \\ \gamma_3 &= \sigma_z, \\ \gamma_4 &= \rho_x\sigma_x, \\ \gamma_5 &= \rho_z\sigma_x. \end{aligned} \quad (24)$$

For odd-parity pairing,

$$C = \tau_x K, \quad P = \tau_z \sigma_z, \quad T = K, \quad (25)$$

the 8×8 BdG Hamiltonian is

$$\begin{aligned} H(\mathbf{k}) = & -\mu(\mathbf{k})\tau_z + f_1(\mathbf{k})\tau_z\rho_y\sigma_x + f_2(\mathbf{k})\tau_z\sigma_y + f_3(\mathbf{k})\tau_z\sigma_z \\ & + m_1(\mathbf{k})\tau_z\rho_z + m_2(\mathbf{k})\tau_z\rho_x + m_3(\mathbf{k})\tau_z\rho_x\sigma_z + m_4(\mathbf{k})\tau_z\rho_z\sigma_z + m_5(\mathbf{k})\tau_z\rho_x\sigma_y + m_6(\mathbf{k})\tau_z\rho_z\sigma_y \\ & + \Delta_1(\mathbf{k})\tau_y + \Delta_2(\mathbf{k})\tau_y\rho_y\sigma_x + \Delta_3(\mathbf{k})\tau_y\sigma_y + \Delta_4(\mathbf{k})\tau_y\sigma_z \\ & + \Delta_5(\mathbf{k})\tau_y\rho_z + \Delta_6(\mathbf{k})\tau_y\rho_x + \Delta_7(\mathbf{k})\tau_y\rho_x\sigma_z + \Delta_8(\mathbf{k})\tau_y\rho_z\sigma_z + \Delta_9(\mathbf{k})\tau_y\rho_x\sigma_y + \Delta_{10}(\mathbf{k})\tau_y\rho_z\sigma_y \\ = & f_1(\mathbf{k})\Gamma_1 + f_2(\mathbf{k})\Gamma_2 + f_3(\mathbf{k})\Gamma_3 + \Delta_1(\mathbf{k})\Gamma_4 \\ & + m_1(\mathbf{k})\Gamma_{237} + m_2(\mathbf{k})\Gamma_{236} - m_3(\mathbf{k})\Gamma_{137} + m_4(\mathbf{k})\Gamma_{136} - m_5(\mathbf{k})\Gamma_{127} + m_6(\mathbf{k})\Gamma_{126} \\ & + \Delta_2(\mathbf{k})\Gamma_{15} + \Delta_3(\mathbf{k})\Gamma_{25} + \Delta_4(\mathbf{k})\Gamma_{35} + \mu(\mathbf{k})\Gamma_{45} \\ & + \Delta_5(\mathbf{k})\Gamma_{146} - \Delta_6(\mathbf{k})\Gamma_{147} + \Delta_7(\mathbf{k})\Gamma_{246} + \Delta_8(\mathbf{k})\Gamma_{247} - \Delta_9(\mathbf{k})\Gamma_{346} - \Delta_{10}(\mathbf{k})\Gamma_{347}, \end{aligned} \quad (26)$$

where

$$\begin{aligned} \Delta_{i=1,4,5,6,7,8}(\mathbf{k}) &= -\Delta_{i=1,4,5,6,7,8}(-\mathbf{k}), \\ \Delta_{i=2,3,9,10}(\mathbf{k}) &= +\Delta_{i=2,3,9,10}(-\mathbf{k}), \end{aligned} \quad (27)$$

and we define

$$\begin{aligned} \Gamma_1 &= \tau_z\rho_y\sigma_x, \\ \Gamma_2 &= \tau_z\sigma_y, \\ \Gamma_3 &= \tau_z\sigma_z, \\ \Gamma_4 &= \tau_y, \\ \Gamma_5 &= \tau_x, \\ \Gamma_6 &= \tau_z\rho_x\sigma_x, \\ \Gamma_7 &= \tau_z\rho_z\sigma_x. \end{aligned} \quad (28)$$

C. Three-band normal state and odd-parity pairing

We consider the following representations of P and T

$$P = 1, \quad T = K, \quad (29)$$

which is relevant for the Kagome lattice we study below. The most general form of the 3×3 normal state Hamiltonian is then

$$h(\mathbf{k}) = -\mu_1(\mathbf{k})\lambda_0 - \mu_2(\mathbf{k})\lambda_3 - \mu_3(\mathbf{k})\lambda_8 + f_1(\mathbf{k})\lambda_1 + f_2(\mathbf{k})\lambda_4 + f_3(\mathbf{k})\lambda_6, \quad (30)$$

where

$$\begin{aligned} \mu_{i=1,2,3}(\mathbf{k}) &= +\mu_{i=1,2,3}(-\mathbf{k}), \\ f_{i=1,2,3}(\mathbf{k}) &= +f_{i=1,2,3}(-\mathbf{k}). \end{aligned} \quad (31)$$

For odd-parity pairing, symmetry operators are

$$C = \tau_x K, \quad P = \tau_z, \quad T = K, \quad (32)$$

and the 6×6 BdG Hamiltonian symmetric under those operations takes the form of

$$\begin{aligned} H(\mathbf{k}) = & -\mu_1(\mathbf{k})\tau_z\lambda_0 - \mu_2(\mathbf{k})\tau_z\lambda_3 - \mu_3(\mathbf{k})\tau_z\lambda_8 + f_1(\mathbf{k})\tau_z\lambda_1 + f_2(\mathbf{k})\tau_z\lambda_4 + f_3(\mathbf{k})\tau_z\lambda_6 \\ & + \Delta_1(\mathbf{k})\tau_y\lambda_0 + \Delta_2(\mathbf{k})\tau_y\lambda_3 + \Delta_3(\mathbf{k})\tau_y\lambda_8 + \Delta_4(\mathbf{k})\tau_y\lambda_1 + \Delta_5(\mathbf{k})\tau_y\lambda_4 + \Delta_6(\mathbf{k})\tau_y\lambda_6, \end{aligned} \quad (33)$$

where

$$\Delta_{i=1,\dots,6}(\mathbf{k}) = -\Delta_{i=1,\dots,6}(-\mathbf{k}). \quad (34)$$

IV. TIGHT-BINDING MODELS

We demonstrate our theory by using simple tight-binding models defined on rectangular or orthorhombic lattices. We construct three models in which the normal states are a Dirac semimetal in 2D, a nodal line semimetal in 3D, and a monopole nodal line semimetal in 3D, respectively. We show that, when an odd-parity superconducting pairing is introduced, the three nodal semimetals turn into a second-order topological superconductor in 2D, a monopole nodal line superconductor in 3D, and a third-order topological superconductor in 3D, respectively.

A. Dirac semimetal and second-order topological superconductor in two dimensions

First, let us consider a 2D Dirac semimetal described by the nearest-neighbor tight-binding Hamiltonian

$$\hat{h} = \hat{h}_\mu + \hat{h}_t = - \sum_{i,\sigma} \mu_\sigma c_{i,\sigma}^\dagger c_{i,\sigma} - \sum_{\langle ij \rangle; \sigma, \sigma'} t_{i,\sigma;j,\sigma'} c_{i,\sigma}^\dagger c_{j,\sigma'}, \quad (35)$$

where $\sigma = s, p_x$ labels the orbital degrees of freedom. In momentum space, we have

$$h = -\mu + 2t \sin k_x \sigma_y + (M - 2t \cos k_x - 2t \cos k_y) \sigma_z, \quad (36)$$

where $\sigma_{y,z}$ are the Pauli matrices for orbital degrees of freedom with $\uparrow (\downarrow)$ indicating a s (p_x) orbital.

$$\begin{aligned} \mu &= \frac{1}{2} (\mu_s + \mu_{p_x}), \\ M &= -\frac{1}{2} (\mu_s - \mu_{p_x}) \\ t &= t_{ss} = -t_{p_x p_x} = t_{sp_x}. \end{aligned} \quad (37)$$

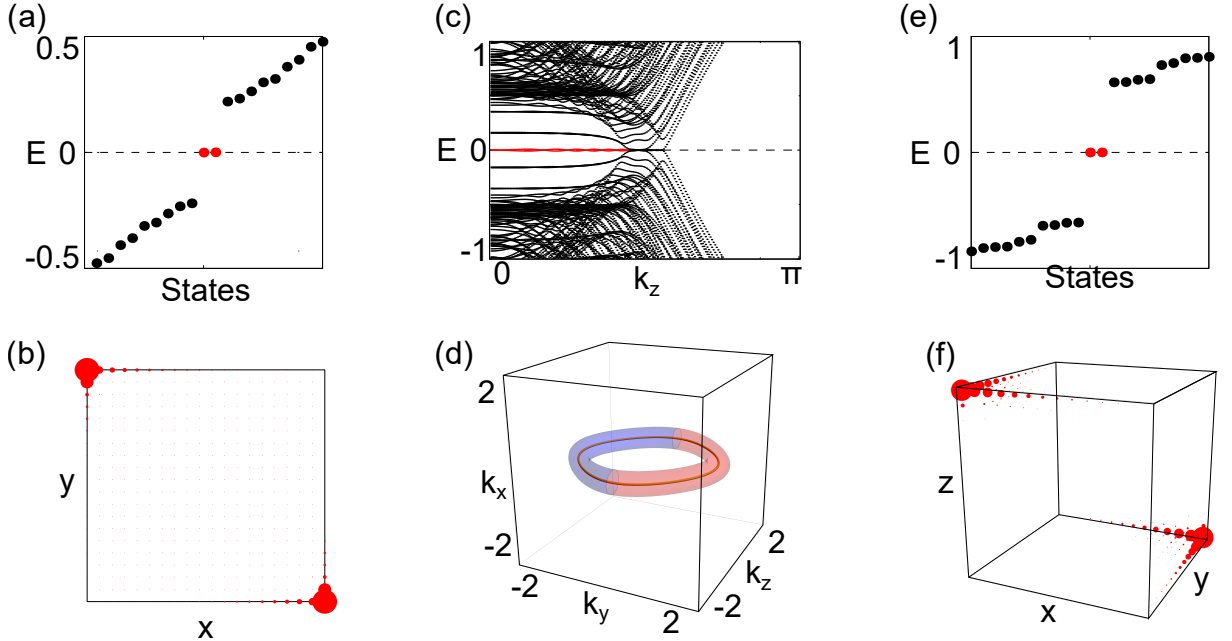


FIG. 1. Higher-order topological superconductivity. (a,b) Zero modes and boundary Majorana states of a two-dimensional second-order topological superconductor described in Eq. (40). Here $t = 1$, $\mu = 0.2$, $M = 2$, and $\Delta_{1,3}(\mathbf{k}) = \sum_{i=x,y} (\Delta_{i,ss}^V \pm \Delta_{i,p_x p_x}^V) \sin k_i$, and $\Delta_2(\mathbf{k}) = \Delta^U$, where $\Delta_{x,ss}^V = \Delta_{x,p_x p_x}^V = 0$, $\Delta_{y,ss}^V = \Delta_{y,p_x p_x}^V = 0.5$, and $\Delta^U = 0.5$, and a 20×20 lattice is considered. (c,d) Zero modes and nodal lines of a monopole nodal line superconductor described in Eq. (40). We take $t = 1$, $M = 4$, $\mu = 0.2$, and $\Delta_{1,3}(\mathbf{k}) = \sum_{i=x,y,z} (\Delta_{i,ss}^V \pm \Delta_{i,p_x p_x}^V) \sin k_i$, and $\Delta_2(\mathbf{k}) = \Delta^U$, where $\Delta_{x,ss}^V = \Delta_{x,p_x p_x}^V = \Delta_{z,ss}^V = \Delta_{z,p_x p_x}^V = 0$, $\Delta_{y,ss}^V = \Delta_{y,p_x p_x}^V = 0.2$, and $\Delta^U = 0$, and a lattice with 20×20 unit cells along x and y in (c). In (d), the torus indicates the Fermi surface enclosing a nodal line (thick gold line) in the normal state. The blue (red) color indicates the region where the pairing function has positive (negative) sign. Two monopole nodal loops appear at the intersection, where the pairing function changes its sign. (e,f) Zero modes and boundary Majorana states of a three-dimensional third-order topological superconductor described in Eq. (47). We take $t = 1$, $\mu = 0.2$, $M = 4$, $m_1 = m_2 = \Delta_1 = \Delta_2 = \Delta_3 = 0.5$ on the $14 \times 14 \times 14$ lattice.

The Hamiltonian is symmetric under $P = \sigma_z$, $T = K$, $M_x = \sigma_z$, $M_y = 1$, $M_z = 1$, where $M_{i=x,y,z}$ indicates a mirror operator that flips the sign of the i -th coordinate. The energy eigenvalues are $E(\mathbf{k}) = -\mu \pm \sqrt{4t^2 \sin^2 k_x + (M - 2t \cos k_x - 2t \cos k_y)^2}$ which exhibit two Dirac points at $(k_x, k_y) = (0, \pm \cos^{-1}[(M/t - 2)/2])$ when $0 < M/t < 4$ at the energy $E = -\mu$.

To induce superconductivity, we consider the following interaction term

$$H_{\text{int}} = -U \sum_{i,\sigma,\sigma'} n_{i,\sigma} n_{i,\sigma'} - V \sum_{\langle i,j \rangle, \sigma} n_{i,\sigma} n_{j,\sigma}, \quad (38)$$

where U indicates the on-site interorbital interaction and V denotes the intraorbital interaction between nearest-neighbor sites. We treat H_{int} within the mean field approximation. Although we focus only inversion symmetry, for a systematic analysis of the lattice model, let us first organize the odd-parity pairing in terms of the irreducible representations of the D_{2h} symmetry group as

$$\begin{aligned} B_{2u} &: -i(\Delta_{y,ss}^V + \Delta_{y,p_x p_x}^V) \sin k_y - i(\Delta_{y,ss}^V - \Delta_{y,p_x p_x}^V) \sin k_y \sigma_z, \\ B_{3u} &: -i(\Delta_{x,ss}^V + \Delta_{x,p_x p_x}^V) \sin k_x - i(\Delta_{x,ss}^V - \Delta_{x,p_x p_x}^V) \sin k_x \sigma_z + i\Delta^U \sigma_y, \end{aligned} \quad (39)$$

where B_{2u} has parity $(+, -, +)$ under (M_x, M_y, M_z) , and B_{3u} has parity $(-, +, +)$ under (M_x, M_y, M_z) . The B_{2u} pairing fully opens the gap. On the other hand, the B_{3u} pairing generates four nodes because the intersection of Fermi surfaces and the $k_x = 0$ plane are the crossing points between two bands with different M_x eigenvalues in the BdG spectrum (by the same argument applied to odd-parity pairing, the particle sector and the hole sector in the Nambu space have opposite M_x eigenvalues since B_{3u} is an odd- M_x pairing). Accordingly, we need to include nonvanishing B_{2u} pairing to open the gap. In general the BdG Hamiltonian takes the form

$$\begin{aligned} H_{\text{BdG}}(\mathbf{k}) &= -\mu \tau_z + 2t \sin k_x \tau_z \sigma_y + (M - 2t \cos k_x - 2t \cos k_y) \tau_z \sigma_z \\ &\quad + \Delta_1(\mathbf{k}) \sin k_y \tau_y + \Delta_2(\mathbf{k}) \tau_y \sigma_y + \Delta_3(\mathbf{k}) \sin k_y \tau_y \sigma_z, \end{aligned} \quad (40)$$

where $\tau_{i=x,y,z}$ are the Pauli matrices for the Nambu space, $\Delta_{1,3}(\mathbf{k}) = \sum_{i=x,y} (\Delta_{i,ss}^V \pm \Delta_{i,p_x p_x}^V) \sin k_i$, and $\Delta_2(\mathbf{k}) = \Delta^U$. We take $t = 1$, $\mu = 0.2$, $M = 2$, $\Delta_{x,ss}^V = \Delta_{x,p_x p_x}^V = 0$, $\Delta_{y,ss}^V = \Delta_{y,p_x p_x}^V = 0.5$, and $\Delta^U = 0.5$, and consider a 20×20 lattice for numerical calculations. The results in Fig. 1(a,b) show two zero modes localized at two corners.

B. Nodal line semimetal and second-order topological nodal superconductor in three dimensions

Similalry, we can construct the Hamiltonian for a 3D nodal line semimetal as

$$h(\mathbf{k}) = -\mu + 2t \sin k_x \sigma_y + (M - 2t \cos k_x - 2t \cos k_y - 2t \cos k_z) \sigma_z, \quad (41)$$

which can be considered as a vertical stacking of 2D Dirac semimetals with an additional hopping along the z direction. The energy eigenvalues are $E(\mathbf{k}) = -\mu \pm \sqrt{4t^2 \sin^2 k_x + M_{\mathbf{k}}^2}$, where $M_{\mathbf{k}} = M - 2t \cos k_x - 2t \cos k_y - 2t \cos k_z$. A single nodal loop surrounding the Γ point appears in the $k_x = 0$ plane at the energy $E = -\mu$ when $2 < M/t < 6$. When $|\mu|$ is smaller than the bandwidth, the Fermi surface is torus-shaped. If we include on-site interorbital U and nearest-neighbor intraorbital V Coulomb interactions as in two dimensions, odd-parity pairing terms are organized into the D_{2h} irreducible representations as

$$\begin{aligned} B_{1u} &: -i(\Delta_{z,ss}^V + \Delta_{z,p_x p_x}^V) \sin k_z - i(\Delta_{z,ss}^V - \Delta_{z,p_x p_x}^V) \sin k_z \sigma_z, \\ B_{2u} &: -i(\Delta_{y,ss}^V + \Delta_{y,p_x p_x}^V) \sin k_y - i(\Delta_{y,ss}^V - \Delta_{y,p_x p_x}^V) \sin k_y \sigma_z, \\ B_{3u} &: -i(\Delta_{x,ss}^V + \Delta_{x,p_x p_x}^V) \sin k_x - i(\Delta_{x,ss}^V - \Delta_{x,p_x p_x}^V) \sin k_x \sigma_z + i\Delta^U \sigma_y, \end{aligned} \quad (42)$$

where B_{1u} , B_{2u} , and B_{3u} has parity $(+, +, -)$, $(+, -, +)$, and $(-, +, +)$ under (M_x, M_y, M_z) , respectively. The relevant BdG Hamiltonian is given by

$$\begin{aligned} H_{\text{BdG}}(\mathbf{k}) &= -\mu \tau_z + 2t \sin k_x \tau_z \sigma_y + (M - 2t \cos k_x - 2t \cos k_y - 2t \cos k_z) \tau_z \sigma_z \\ &\quad + \Delta_1(\mathbf{k}) \sin k_y \tau_y + \Delta_2(\mathbf{k}) \tau_y \sigma_y + \Delta_3(\mathbf{k}) \sin k_y \tau_y \sigma_z, \end{aligned} \quad (43)$$

with $\Delta_{1,3}(\mathbf{k}) = \sum_{i=x,y,z} (\Delta_{i,ss}^V \pm \Delta_{i,p_x p_x}^V) \sin k_i$ and $\Delta_2(\mathbf{k}) = \Delta^U$. We take $t = 1$, $M = 4$, $\mu = 0.2$ with a B_{2u} pairing: $\Delta_{x,ss}^V = \Delta_{x,p_x p_x}^V = \Delta_{z,ss}^V = \Delta_{z,p_x p_x}^V = 0$, $\Delta_{y,ss}^V = \Delta_{y,p_x p_x}^V = 0.2$, and $\Delta^U = 0$ for numerical calculations. The spectrum of the BdG Hamiltonian is gapless at $k_y = 0$ on the torus Fermi surface due to the sign change of

the pairing term. The nodal structure can be seen explicitly from the energy eigenvalues of the BdG Hamiltonian given by $\xi(\mathbf{k}) = \pm \sqrt{(\Delta_{y,ss}^V + \Delta_{y,p_x p_x}^V)^2 \sin^2 k_y + \left(\sqrt{4t^2 \sin^2 k_x + M_{\mathbf{k}}^2} - \mu\right)^2}$. Fig. 1(d) shows the corresponding Fermi surface of a torus shape and the location of nodes. Interestingly, the two nodal loops at $k_y = 0$ are linked with the nodal loop of the normal state, which appears as the crossing between the occupied bands of the BdG Hamiltonian. This *linking structure* indicates that the zero-energy nodes carry nontrivial monopole charges [2]. To see the higher-order topology of this phase, we consider the open boundary condition with 20×20 unit cells along x and y and the periodic boundary condition along the z direction. The spectrum shown in Fig. 1(c) reveals zero modes in a finite range of k_z , which is inside the nodal loop of the normal state, and they originate from the nontrivial second Stiefel-Whitney number in the range of k_z . We also have two monopole nodal lines for pairing in the B_{1u} representation, which are now on the $k_z = 0$ plane. Let us note that, for pairing in the B_{3u} representation, however, two trivial loops are created at the $k_x = 0$ plane. Although $\nu_2^{\text{BdG}} = 1$, monopole nodal line do not exist. It is basically because any inversion-invariant 2D subBrillouin zone passing through the $\mathbf{k} = 0$ is gapless.

C. Monopole nodal line semimetal and third-order topological superconductor in three dimensions

Finally, let us consider the odd-parity superconductivity of a doped monopole nodal line semimetal. The nearest-tight-binding Hamiltonian for the normal state is

$$\hat{h} = \hat{h}_\mu + \hat{h}_t = - \sum_{i,\tau} \mu_\tau c_{i,\tau}^\dagger c_{i,\tau} - \sum_{\langle ij \rangle; \tau, \tau'} t_{i,\tau; j, \tau'} c_{i,\tau}^\dagger c_{j, \tau'}, \quad (44)$$

where $\tau = s, p_x, p_y, d_{xy}$ labels orbital degrees of freedom. In momentum space,

$$h(\mathbf{k}) = -\mu + 2t \sin k_x \rho_y \sigma_x + 2t \sin k_y \sigma_y + (M - 2t \cos k_x - 2t \cos k_y - 2t \cos k_z) \sigma_z + m_1 \rho_z + m_2 \rho_z \sigma_z \quad (45)$$

where ρ and σ are Pauli matrices for orbital degrees of freedom. Here, the basis states are $(s, p_y, d_{xy}, p_x)^T$, and

$$\begin{aligned} \mu &= \frac{1}{4} (\mu_s + \mu_{p_y} + \mu_{d_{xy}} + \mu_{p_x}), \\ M &= -\frac{1}{4} (\mu_s - \mu_{p_y} + \mu_{d_{xy}} - \mu_{p_x}), \\ m_1 &= -\frac{1}{4} (\mu_s + \mu_{p_y} - \mu_{d_{xy}} - \mu_{p_x}), \\ m_2 &= -\frac{1}{4} (\mu_s - \mu_{p_y} - \mu_{d_{xy}} + \mu_{p_x}), \\ t &= t_{ss} = -t_{p_y p_y} = t_{d_{xy} d_{xy}} = -t_{p_x p_x} = t_{sp_x} = t_{d_{xy} p_y} = t_{sp_y} = t_{d_{xy} p_x}. \end{aligned} \quad (46)$$

The Hamiltonian is symmetric under $P = \sigma_z$, $T = K$, $M_x = \rho_z$, $M_y = \rho_z \sigma_z$, $M_z = 1$. When $m_1 = m_2 = 0$ and $2 < M/t < 6$, this Hamiltonian describes two Dirac points at $(k_x, k_y, k_z) = (0, 0, \pm \cos^{-1}[(M-4)/2t])$, which correspond to a particular limit of a monopole nodal line shrunk to a point. It can be seen from the energy spectrum $E(\mathbf{k}) = -\mu \pm \sqrt{4t^2 \sin^2 k_x + 4t^2 \sin^2 k_y + M_{\mathbf{k}}^2}$, where $M_{\mathbf{k}} = M - 2t \cos k_x - 2t \cos k_y - 2t \cos k_z$. Nonzero m_1 and m_2 make the monopole nodal lines have a finite size. When interorbital onsite and intraorbital nearest-neighbor Coulomb interactions are considered, pairing functions can be classified to B_{1u} , B_{2u} , or B_{3u} representation of D_{2h} as we did above, and the B_{1u} pairing opens the full gap. Therefore we consider the B_{1u} pairing with two additional mirror-breaking pairing Δ_9 and Δ_{10} needed to obtain well-localized corner states. Adding those superconducting pairing, we have

$$\begin{aligned} H_{\text{BdG}}(\mathbf{k}) &= -\mu \Gamma_{45} + 2t \sin k_x \Gamma_1 + 2t \sin k_y \Gamma_2 + (M - 2t \cos k_x - 2t \cos k_y - 2t \cos k_z) \Gamma_3 \\ &\quad + m_1 \Gamma_{136} + m_2 \Gamma_{237} + \Delta_1 \sin k_z \Gamma_4 + \Delta_4 \sin k_z \Gamma_{35} \\ &\quad + \Delta_5 \sin k_z \Gamma_{146} + \Delta_8 \sin k_z \Gamma_{247} - \Delta_9 \Gamma_{346} - \Delta_{10} \Gamma_{347}, \end{aligned} \quad (47)$$

where $\Gamma_1 = \tau_z \rho_y \sigma_x$, $\Gamma_2 = \tau_z \sigma_y$, $\Gamma_3 = \tau_z \sigma_z$, $\Gamma_4 = \tau_y$, $\Gamma_5 = \tau_x$, $\Gamma_6 = \tau_z \rho_x \sigma_x$, $\Gamma_7 = \tau_z \rho_z \sigma_x$, $\Gamma_{ij} = -i\Gamma_i \Gamma_j$, and $\Gamma_{ijk} = -i\Gamma_i \Gamma_j \Gamma_k$. The spectrum is fully gapped when $t = 1$, $\mu = 0.2$, $M = 4$, $m_1 = m_2 = \Delta_1 = \Delta_9 = \Delta_{10} = 0.5$, and $\Delta_4 = \Delta_5 = \Delta_8 = 0$. Fig. 1(e,f) shows the presence of zero modes localized at two corners.

V. MORE ON TIGHT-BINDING MODELS IN TWO DIMENSIONS

A. Hexagonal lattice

1. Normal state

We begin with the nearest-neighbor tight-binding model.

$$\hat{h} = \hat{h}_\mu + \hat{h}_t = -\mu \sum_i c_i^\dagger c_i - t \sum_{\langle ij \rangle} c_i^\dagger c_j \quad (48)$$

In momentum space, we have

$$\begin{aligned} h(\mathbf{k}) &= \begin{pmatrix} -t(e^{i\mathbf{k}\cdot\mathbf{a}_1} + e^{i\mathbf{k}\cdot\mathbf{a}_2} + e^{i\mathbf{k}\cdot\mathbf{a}_3}) & \mu \\ \mu & -t(e^{-i\mathbf{k}\cdot\mathbf{a}_1} + e^{-i\mathbf{k}\cdot\mathbf{a}_2} + e^{-i\mathbf{k}\cdot\mathbf{a}_3}) \end{pmatrix} \\ &= \mu - [t \cos(\mathbf{k} \cdot \mathbf{a}_1) + t \cos(\mathbf{k} \cdot \mathbf{a}_2) + t \cos(\mathbf{k} \cdot \mathbf{a}_3)] \sigma_x - [t \sin(\mathbf{k} \cdot \mathbf{a}_1) + t \sin(\mathbf{k} \cdot \mathbf{a}_2) + t \sin(\mathbf{k} \cdot \mathbf{a}_3)] \sigma_y \\ &= \mu - (t \cos k_1 + t \cos k_2 + t \cos k_3) \sigma_x - (t \sin k_1 + t \sin k_2 + t \sin k_3) \sigma_y \end{aligned} \quad (49)$$

where

$$\begin{aligned} k_1 = \mathbf{k} \cdot \mathbf{a}_1 &= \frac{1}{\sqrt{3}} k_y, \\ k_2 = \mathbf{k} \cdot \mathbf{a}_2 &= -\frac{1}{2} k_x - \frac{1}{2\sqrt{3}} k_y \\ k_3 = \mathbf{k} \cdot \mathbf{a}_3 &= \frac{1}{2} k_x - \frac{1}{2\sqrt{3}} k_y. \end{aligned} \quad (50)$$

It has symmetries under

$$T = K, \quad C_3 = 1, \quad M_z = 1, \quad M_x = 1, \quad M_y = \sigma_x, \quad P = \sigma_x, \quad (51)$$

where the crystalline symmetry operations form the D_{6h} group. The Hamiltonian has the form of

$$h(\mathbf{k}) = -\mu(\mathbf{k}) + f_1(\mathbf{k})\sigma_x + f_2(\mathbf{k})\sigma_y, \quad (52)$$

where

$$\begin{aligned} \mu(\mathbf{k}) &= \mu, \\ f_1(\mathbf{k}) &= -t \cos k_1 - t \cos k_2 - t \cos k_3, \\ f_2(\mathbf{k}) &= -t \sin k_1 - t \sin k_2 - t \sin k_3. \end{aligned} \quad (53)$$

Two Dirac points appear at $K = (\pi/\sqrt{3}, \pi)$ and $K' = (-\pi/\sqrt{3}, \pi)$ points at $E = -\mu$.

$$C = \tau_x K, \quad P = \tau_z \sigma_x. \quad (54)$$

2. Superconducting state

Let us consider Coulomb interactions. There is no on-site Coulomb interaction because of the Fermi statistics. We consider the nearest and the next-nearest neighbor Coulomb interactions.

$$\begin{aligned} H_{\text{int}} &= -U \sum_{\langle i,j \rangle} n_i n_j - V \sum_{\langle\langle i,j \rangle\rangle} n_i n_j \\ &\approx \sum_{\langle i,j \rangle} \left[c_i^\dagger c_j^\dagger \Delta_{ij}^U + c_j c_i \Delta_{ij}^{U*} - U^{-1} \Delta_{ij}^{U*} \Delta_{ij}^U \right] + \sum_{\langle\langle i,j \rangle\rangle} \left[c_i^\dagger c_j^\dagger \Delta_{ij}^V + c_j c_i \Delta_{ij}^{V*} - V^{-1} \Delta_{ij}^{V*} \Delta_{ij}^V \right] \\ &= \sum_{\mathbf{k}} \left[c_{A\mathbf{k}}^\dagger c_{B-\mathbf{k}}^\dagger \Delta_{AB}^U(\mathbf{k}) + c_{A-\mathbf{k}} c_{B\mathbf{k}} \Delta_{AB}^{U*}(\mathbf{k}) + c_{A\mathbf{k}}^\dagger c_{B-\mathbf{k}}^\dagger \Delta_{AB}^V(\mathbf{k}) + c_{A-\mathbf{k}} c_{B\mathbf{k}} \Delta_{AB}^{V*}(\mathbf{k}) \right] + \text{const}, \end{aligned} \quad (55)$$

where $\Delta_{ij}^{U(V)} = -\Delta_{ji}^{U(V)} \equiv \Delta^{U(V)}$, A and B are two sublattice indices, and $c_i = \frac{1}{\sqrt{N}} \sum_{\mathbf{k}} c_{A/B, \mathbf{k}} e^{i\mathbf{k} \cdot \mathbf{r}_i}$ depending on whether \mathbf{r}_i is in the A or B sublattice.

$$\begin{aligned} \Delta^U(\mathbf{k}) &= \Delta^U \sum_{i=1}^3 \begin{pmatrix} 0 & e^{-i\mathbf{k} \cdot \mathbf{a}_i} \\ -e^{i\mathbf{k} \cdot \mathbf{a}_i} & 0 \end{pmatrix} \\ &= -i\Delta^U \left\{ [\cos(\mathbf{k} \cdot \mathbf{a}_1) + \cos(\mathbf{k} \cdot \mathbf{a}_2) + \cos(\mathbf{k} \cdot \mathbf{a}_3)]\sigma_y + [\sin(\mathbf{k} \cdot \mathbf{a}_1) + \sin(\mathbf{k} \cdot \mathbf{a}_2) + \sin(\mathbf{k} \cdot \mathbf{a}_3)]\sigma_x \right\} \\ \Delta^V(\mathbf{k}) &= -2i\Delta^V \sum_{i=1}^3 \begin{pmatrix} \sin(\mathbf{k} \cdot \mathbf{b}_i) & 0 \\ 0 & \sin(\mathbf{k} \cdot \mathbf{b}_i) \end{pmatrix} \\ &= -2i\Delta^V [\sin(\mathbf{k} \cdot \mathbf{b}_1) + \sin(\mathbf{k} \cdot \mathbf{b}_2) + \sin(\mathbf{k} \cdot \mathbf{b}_3)]. \end{aligned} \quad (56)$$

$\Delta^U(\mathbf{k})$ and $\Delta^V(\mathbf{k})$ are in the B_{2u} and B_{1u} irreducible representations of the D_{6h} symmetry group, respectively. The B_{2u} pairing has two nodes at $k_y = 0$ because it is odd under M_y , while B_{1u} pairing open the full gap. Accordingly, the B_{1u} pairing is energetically favored.

The corresponding BdG Hamiltonian for the B_{1u} pairing is

$$H = -\mu(\mathbf{k})\tau_z + f_1(\mathbf{k})\tau_z\sigma_x + f_2(\mathbf{k})\tau_z\sigma_y + \Delta_1(\mathbf{k})\tau_y + \Delta_2(\mathbf{k})\tau_y\sigma_x + \Delta_3(\mathbf{k})\tau_y\sigma_y, \quad (57)$$

where $\Delta_1(\mathbf{k}) = \Delta^V(\mathbf{k})$, and $\Delta_2(\mathbf{k}) = \Delta_3(\mathbf{k}) = 0$. The BdG Hamiltonian is symmetric under

$$C = \tau_x K, \quad T = K, \quad C_3 = 1, \quad M_z = 1, \quad M_x = \tau_z, \quad M_y = \sigma_x, \quad P = \tau_z\sigma_x, \quad (58)$$

Table. II shows that $\nu_2^{\text{BdG}} = 1$ for $\mu = 0.2, t = 1, \Delta^V = 0.05$, i.e., we have a second-order topological superconductor.

TRIM	(0, 0)	$(\pi, \pi/\sqrt{3})$	$(-\pi, \pi/\sqrt{3})$	$(0, 2\pi/\sqrt{3})$
parity	(+, +)	(-, -)	(-, -)	(-, -)

TABLE II. Parity eigenvalues of the occupied states of the BdG Hamiltonian in Eq. (57). $\mu = 0.2, t = 1, \Delta^V = 0.05$.

B. Kagome lattice

1. Normal state

The nearest-neighbor tight-binding model on the Kagome lattice features one exactly flat band and other two bands crossing at the K points, forming two Dirac points. Superconductivity on the Kagome Lattice has been studied in the context of the large correlation effect due to the flat band. Here, we consider the superconductivity of spin-polarized electrons at the filling near the Dirac points.

The nearest-neighbor tight-binding Hamiltonian is given by

$$\hat{h} = \hat{h}_\mu + \hat{h}_t = -\mu \sum_i c_i^\dagger c_i - t \sum_{\langle ij \rangle} c_i^\dagger c_j. \quad (59)$$

In momentum space, we have

$$h(\mathbf{k}) = \begin{pmatrix} -\mu & -2t \cos k_1 & -2t \cos k_2 \\ -2t \cos k_1 & -\mu & -2t \cos k_3 \\ -2t \cos k_2 & -2t \cos k_3 & -\mu \end{pmatrix}, \quad (60)$$

where

$$\begin{aligned} k_1 &= \mathbf{k} \cdot \mathbf{a}_1 = \frac{1}{2}k_x, \\ k_2 &= \mathbf{k} \cdot \mathbf{a}_2 = -\frac{1}{4}k_x + \frac{\sqrt{3}}{4}k_y, \\ k_3 &= \mathbf{k} \cdot \mathbf{a}_3 = -\frac{1}{4}k_x - \frac{\sqrt{3}}{4}k_y. \end{aligned} \quad (61)$$

$\mathbf{a}_{i=1,2,3}$ connects nearest neighbor sites. Let us introduce Gell-Mann matrices $\lambda_{i=0,\dots,8}$ for notational convenience.

$$\begin{aligned}\lambda_0 &= \begin{pmatrix} 1 & 0 & 0 \\ 0 & 1 & 0 \\ 0 & 0 & 1 \end{pmatrix}, \quad \lambda_1 = \begin{pmatrix} 0 & 1 & 0 \\ 1 & 0 & 0 \\ 0 & 0 & 0 \end{pmatrix}, \quad \lambda_2 = \begin{pmatrix} 0 & -i & 0 \\ i & 0 & 0 \\ 0 & 0 & 0 \end{pmatrix} \\ \lambda_3 &= \begin{pmatrix} 1 & 0 & 0 \\ 0 & -1 & 0 \\ 0 & 0 & 0 \end{pmatrix}, \quad \lambda_4 = \begin{pmatrix} 0 & 0 & 1 \\ 0 & 0 & 0 \\ 1 & 0 & 0 \end{pmatrix}, \quad \lambda_5 = \begin{pmatrix} 0 & 0 & i \\ 0 & 0 & 0 \\ -i & 0 & 0 \end{pmatrix} \\ \lambda_6 &= \begin{pmatrix} 0 & 0 & 0 \\ 0 & 0 & 1 \\ 0 & 1 & 0 \end{pmatrix}, \quad \lambda_7 = \begin{pmatrix} 0 & 0 & 0 \\ 0 & 0 & -i \\ 0 & i & 0 \end{pmatrix}, \quad \lambda_8 = \frac{1}{\sqrt{3}} \begin{pmatrix} 1 & 0 & 0 \\ 0 & 1 & 0 \\ 0 & 0 & -2 \end{pmatrix}.\end{aligned}\quad (62)$$

Using Gell-Mann matrices, we can write the Hamiltonian as

$$h(\mathbf{k}) = -\mu\lambda_0 - 2t(\cos k_1\lambda_1 + \cos k_2\lambda_4 + \cos k_3\lambda_6). \quad (63)$$

Two Dirac points appear at $K = (\pi/\sqrt{3}, \pi)$ and $K' = (-\pi/\sqrt{3}, \pi)$ points at $E = -t/2 - \mu$. One can see that it has the form of Eq. (30) with $\mu_1 = \mu$, $\mu_2 = \mu_3 = 0$, and $f_{i=1,2,3} = 2t \cos k_{i=1,2,3}$. The Hamiltonian is symmetric under

$$T = K, \quad C_3 = \begin{pmatrix} 0 & 0 & 1 \\ 1 & 0 & 0 \\ 0 & 1 & 0 \end{pmatrix}, \quad M_z = 1, \quad M_x = \begin{pmatrix} 0 & 1 & 0 \\ 1 & 0 & 0 \\ 0 & 0 & 1 \end{pmatrix}, \quad M_y = \begin{pmatrix} 0 & 1 & 0 \\ 1 & 0 & 0 \\ 0 & 0 & 1 \end{pmatrix}, \quad P = 1, \quad (64)$$

where C_3 is the 120° rotation about the z axis, and $M_{i=x,y,z}$ is the mirror operation that flips the $i = x, y, z$ coordinate.

2. Superconducting state

Let us add Coulomb interactions. Since there is no on-site Coulomb interaction due to the Fermi statistics of spin-polarized fermions, we consider the nearest-neighbor interaction only.

$$\begin{aligned}H_{\text{int}} &= -U \sum_{\langle i,j \rangle} n_i n_j \\ &\approx \sum_{\langle i,j \rangle} \left[c_i^\dagger c_j^\dagger \Delta_{ij} + c_j c_i \Delta_{ij}^* - U^{-1} \Delta_{ij}^* \Delta_{ij} \right] \\ &= \sum_{\mathbf{k}} \left[c_{A\mathbf{k}}^\dagger c_{B-\mathbf{k}}^\dagger \Delta_{AB}(\mathbf{k}) + c_{A-\mathbf{k}} c_{B\mathbf{k}} \Delta_{AB}^*(\mathbf{k}) \right] + \text{const},\end{aligned}\quad (65)$$

where $A, B = 1, 2, 3$ are sublattice indices, and

$$\begin{aligned}\Delta(\mathbf{k}) &= -2i\Delta \begin{pmatrix} 0 & \sin(\mathbf{k} \cdot \mathbf{a}_1) & \sin(\mathbf{k} \cdot \mathbf{a}_2) \\ \sin(\mathbf{k} \cdot \mathbf{a}_1) & 0 & \sin(\mathbf{k} \cdot \mathbf{a}_3) \\ \sin(\mathbf{k} \cdot \mathbf{a}_2) & \sin(\mathbf{k} \cdot \mathbf{a}_3) & 0 \end{pmatrix} \\ &= -2i\Delta(\sin k_1\lambda_1 + \sin k_2\lambda_4 + \sin k_3\lambda_6).\end{aligned}\quad (66)$$

This pairing matrix belongs to the B_{1u} irreducible representation of the D_{6h} group, i.e., it is invariant under C_{3z} and has parity $(-, +, +)$ under mirror (M_x, M_y, M_z) . It opens the full gap on the Fermi surfaces. The BdG Hamiltonian has the form

$$\begin{aligned}H(\mathbf{k}) &= -\mu\tau_z\lambda_0 - 2t(\cos k_1\tau_z\lambda_1 + \cos k_2\tau_z\lambda_4 + \cos k_3\tau_z\lambda_6) \\ &\quad + 2\Delta \sin k_1\tau_y\lambda_1 + 2\Delta \sin k_2\tau_y\lambda_4 + 2\Delta \sin k_3\tau_y\lambda_6.\end{aligned}\quad (67)$$

It corresponds to Eq. (33) with $\mu_1 = \mu$, $f_{i=1,2,3} = -2t \cos k_{i=1,2,3}$, $\mu_2 = \mu_3 = \Delta_1 = \Delta_2 = \Delta_3 = 0$, and $\Delta_{i=4,5,6} = 2\Delta \sin k_{i=4,5,6}$.

Table. III shows the parity eigenvalues of the occupied states of the BdG Hamiltonian for $t = 1$, $\mu = -0.3$, and $\Delta = 0.05$. Although we introduce odd-parity pairing in a doped Dirac semimetal, we have $\nu_2^{\text{BdG}} = 0 \pmod{2}$. This is because the unit cell

in the Kagome lattice is not inversion-invariant (it is inversion-invariant only up to some lattice translation of sublattice sites), which is consistent with our formula Eq. (2).

-
- [1] T. Bzdušek and M. Sigrist, “Robust doubly charged nodal lines and nodal surfaces in centrosymmetric systems,” *Phys. Rev. B* **96**, 155105 (2017).
 [2] J. Ahn, D. Kim, Y. Kim, and B.-J. Yang, “Band topology and linking structure of nodal line semimetals with Z_2 monopole charges,” *Phys. Rev. Lett.* **121**, 106403 (2018).

TRIM	$(0, 0)$	$(\pi, \pi/\sqrt{3})$	$(-\pi, \pi/\sqrt{3})$	$(0, 2\pi/\sqrt{3})$
parity	$(+, -, -)$	$(+, +, -)$	$(+, +, -)$	$(-, -, +)$

TABLE III. Parity eigenvalues of the occupied states of the BdG Hamiltonian in Eq. (67). $t = 1$, $\mu = -0.3$, and $\Delta = 0.05$.